COPPER MINERALIZATION OF THE UPPER MOYA SANDSTONE, CHUPADERO MINES AREA, SOCORRO COUNTY, NEW MEXICO

A Thesis

Presented to

the Faculty of the Department of Geoscience

New Mexico Institute of Mining and Technology

In Partial Fulfillment

of the Requirements for the Degree

Master of Science

by

Michael John Jaworski

September, 1973

TABLE OF CONTENTS

ILLUSTRATIONS

Figures

ABSTRACT

The Chupadero Mines area is located approximately 10 miles southwest from the southern tip of the Los Pinos Mountains, in a northeast-trending fault block of Pennsylvanian and Permian bedrock.

Copper mineralization in the Chupadero Mines area occurs as irregular stratabound deposits which are localized in the sandstone lithofacies of the upper member of the Moya Formation. The dominant copper minerals consist of malachite and azurite and occur as interstitial cements and fracture-fillings. Origin for the upper mineralization in the sandstone lithofacies appears to have been derived from the oxidation and leaching of an overlying cupriferous shale by meteoric waters.

ACKNOWLEDGMENTS

I am greatly indebted to my advisor, Dr. Karl Vonder Linden, and to committee members Dr. Christina Lochman-Balk, Dr. Richard Beane and Dr. Frank Kottlowski, for their patience, guidance and encouragement. I also wish to thank Mr. W. K. Summers for suggesting the problem and Mr. A. B. Baca for information regarding the previous mining in the area and also for allowing me to remove mineralized specimens from his claims at Chupadero Mines. Special thanks go to the New Mexico State Bureau of Mines and Mineral Resources for a research assistantship which enabled me to pursue a graduate degree. I would also like to acknowledge the assistance of Mr. Blair Benner who aided in metallurgical information, and Dr. Marshall Reiter who conducted a thermal well-log test at drill-hole 13 in the Chupadero Mines area. Finally, I would like to express my gratitude to my wife, Mary, my parents, Mr. and Mrs. John Jaworski, and fellow students and friends who aided in many ways during the preparation of this thesis.

INTRODUCTION

Statement of Problem

The purpose of this investigation is to determine the pertinent factors that influenced the localization of stratabound copper mineralization at the Chupadero Mines area.

Location and Accessibility

The Chupadero Mines area is approximately six miles northeast of Socorro in the Loma de las Cañas 7½ minute U.S.G.S. quadrangle, Socorro County, New Mexico (Figure 1). The area studied is comprised of section 26 and the southern portion of section 23 in T. 2 S., R. 1 E.; total area is slightly greater than one square mile.

The study area can be reached by traveling approximately two miles north from Socorro on Interstate 25 to the Escondida exit. Turn east and follow the two-lane paved road to the Escondida Lake turnoff. Again turn east and cross the narrow one-lane bridge over the Rio Grande. From this point the remainder of the traveling will be done on dirt roads. Proceed 1.4 miles in a southeasterly direction until reaching a fork in the road marked by a Bureau of Land Management sign, turn east and travel 3.5 miles to the approximate western margin of the study area.

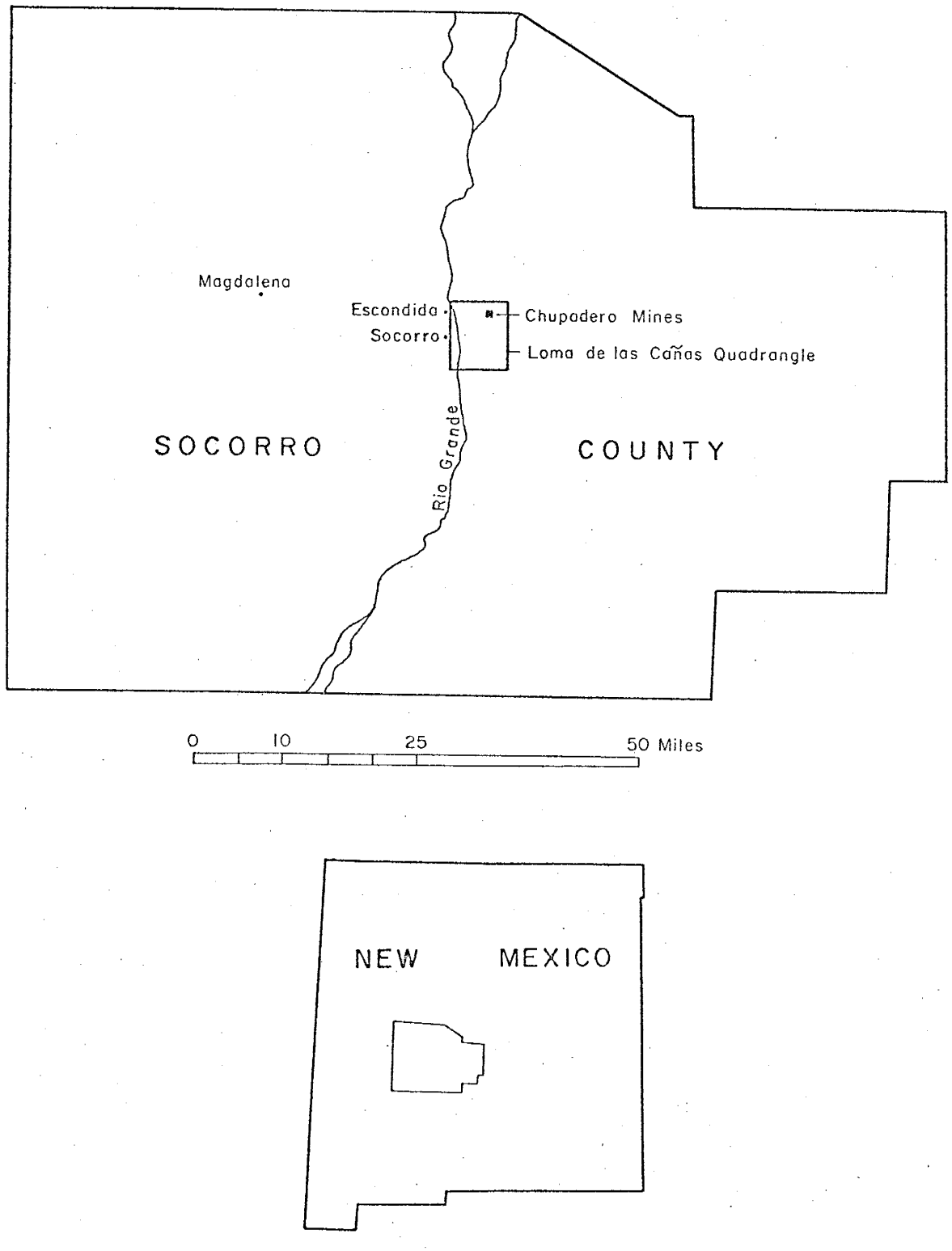

Figure 1. Location map of Chupadero Mines area.

Geologic Setting, Topography, Climate, and Vegetation

The Chupadero Mines area is located approximately 10 miles southwest from the southern tip of the Los Pinos Mountains, in a northeast-trending fault block of Pennsylvanian and Permian sediments. The topographic expression in the study area is of low to moderate relief and has been controlled primarily by faulting (Figure 2). Dip-slopes, ledges and cliffs, created by the more resistant weathering units are the prominent features. Many of the dip-slopes as well as the low topographic areas have been incised by numerous small gullies formed by intermittent streams. These small channels flow into the tributaries of Arroyo de los Pinos which bisects the study area (Figure 2). The climatic conditions in this region are typical of the semi-arid southwest. Generally, warm weather prevails except for several months during the winter, and annual rain-fall averages less than 10 to 11 inches. Sparse vegetation consisting of juniper, sagebrush and a large variety of cacti occur in the area studied. The junipers have a preference for the intermittent stream courses while the sagebrush and cacti grow at random.

Previous Mining

Copper ore, consisting predominately of malachite and azurite in sandstone, was mined from two small open-pits in

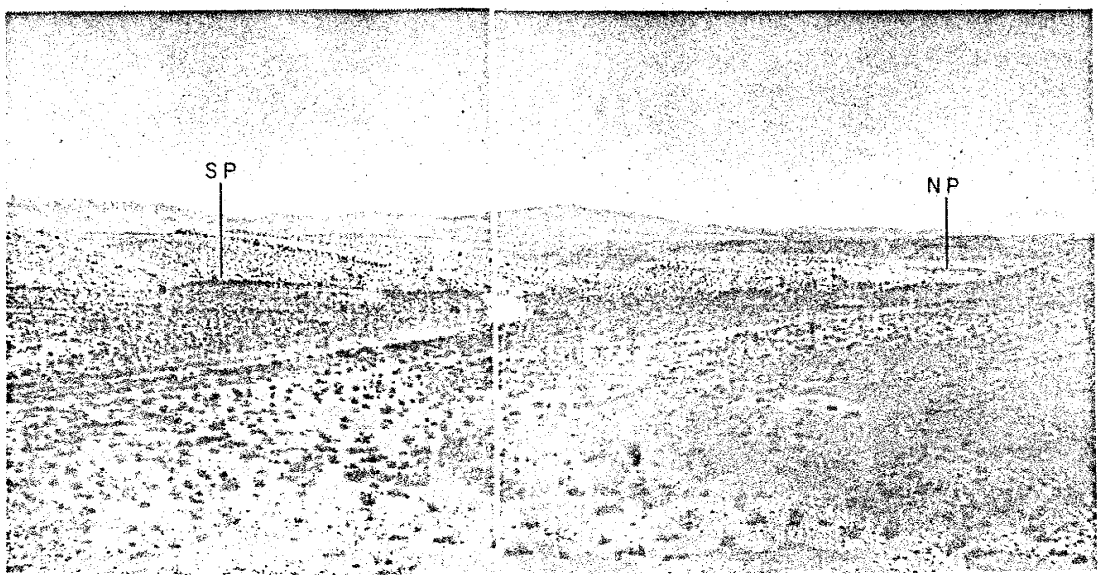

Figure 2. Distant view of the Chupadero Mines area showing the topographic expression in the study area. View to west-northwest. Light-gray to brown hills in the middle distance are upthrown Pennsylvanian strata which strike approximately east-west and dip about 15 degrees to the north. The North and South Pits, near the base of these hills, are located by the vertical arrows. The darker reddish-brown rocks belong to the Abo Formation, with those in the foreground occurring in a northeast-trending graben. A tributary channel of Arroyo de los Pinos dissects the Quaternary Slope Wash deposits which occupy topographic lows in the graben.

the Chupadero Mines area. These pits, designated North Pit and South Pit in this report, are located in the central portion of the mapped area (Plate I and Figure 2). The North Pit was developed along a northeast-trending exposure of mineralized sandstone, adjacent to a prominent northeast-trending fault (Plate I and Figure 3). Additional workings located to the west-southwest of the North Pit include several prospect pits, a shallow vertical shaft and a southeast-trending adit, designated the northern adit. The adit was driven through northwest-dipping bedrock into the mineralized sandstone (Plate I).

The South Pit is a shallow excavation in a mineralized sandstone outcrop located approximately 1500 feet southwest of the North Pit (Plate I and Figure 2). An adit (designated the southern adit) approximately 50 feet in length has been driven into another mineralized sandstone outcrop approximately 100 feet north-northwest of the South Pit. Several small prospect pits are also present in the vicinity of the South Pit.

Approximately 2000 tons of ore averaging two percent copper, were mined from these workings during 1958 to 1960 (A. B. Baca personal communication, 1973). Most of this production was from the North Pit.

Previous Investigations

Lasky (1932, p. 36) briefly described the general

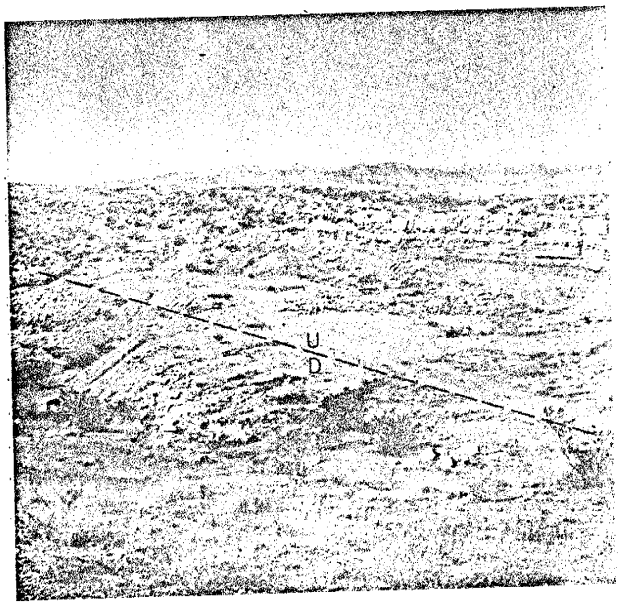

Figure 3. View of North Pit, looking west, with Socorro Mountain and snow-capped Magdalena Mountains in distance. Light-green areas in floor of the pit are exposures of sandstone containing malachite and azurite mineralization. Approximate location of the major fault between the exposed Permian Abo Formation and the Pennsylvanian upper Moya is shown by dashed line.

geology and associated copper mineralization at the Chupadero Mines area.

Wilpolt and Wanek (1951) published a reconnaissance geologic map extending from Socorro eastward to Chupadera Mesa. The Chupadero Mines area lies within the boundaries of this map, but no mention was made of the mineralization.

Soule´ (1956, p. 64) published a circular on "red bed" copper deposits in southeastern Colorado and New Mexico in which he gave a brief description of the geology and mineralization of the Chupadero Mines area.

Hambleton (1959, Plate 1) as part of an investigation in reconstructing paleoenvironments for Missourian strata, presented a stratigraphic section of carbonate sediments measured in section 27 of the Loma de las Cañas 7½ minute quadrangle. This section included bedrock units exposed in the study area.

Rejas (1965) tentatively correlated stratigraphic units found within the northeastern part of the Loma de las Cañas Quadrangle, including the study area, with units designated by Thompson (1942) and Hambleton (1959). He also prepared a geological map of the area at a scale of 1:24,000.

Present Investigation

The present investigation was undertaken as part of an in-situ leaching project initiated by the New Mexico

State Bureau of Mines and Mineral Resources. The geologic portion of this investigation consisted of three phases:

1. Geologic mapping
2. Detailed study of the host rock, including environment of deposition.
3. Analysis to determine the probable genesis and paragenesis of the copper mineralization.

Names of stratigraphic units described by Rejas (1965), which were correlated with the works of Thompson (1942) and Hambleton (1959) were used during this investigation. Rock descriptions were determined from thin sections, drill-hole cores, and also from fresh and weathered surface exposures. A sandstone classification adapted from Koehn (1972, p. 18) was used during the petrographic analysis of the clastic sediments; the terminology used in classifying carbonate rocks was taken from Folk (1968). The G.S.A. Rock Color Chart published in 1963 was used to determined the color descriptions of the rock units. Bed thicknesses of the stratigraphic units were described by the following classification:

fissile: 1/16 inch or less
laminated: 1/16 to 1/4 inch
platey: 1/4 to 1 inch
very thin bedded: 1 to 6 inches
thin bedded: 6 inches to 1 foot
medium bedded: 1 to 2 feet
thick bedded: 2 to 4 feet
very thick bedded: 4 to 6 feet
massive bedded: 6 feet or greater

The geology of the Chupadero Mines area was mapped in detail on colored aerial photographs at a scale of 1:6000. These data then were transferred to a topographic base map having a scale of 1:2400.

Geologic features of the host rock were examined and compared to the characteristics of six possible sedimentary depositional environments. The sedimentary model having the largest number of characteristics in common with the host rock was selected as representing the probable depositional environment.

The suggested genesis and paragenesis of mineralization were determined from field observations and by petrographic study of the host rock and its associated mineralization.

Significant information pertaining to both the depositional environment of the host rock and the copper mineralization was obtained from diamond drill cores recovered during an extensive drilling project sponsored by the New Mexico State Bureau of Mines and Mineral Resources. The well-log descriptions of the exploratory drill-holes are presented in Appendix I.

STRATIGRAPHY

Rock units exposed in the Chupadero Mines area are composed of sediments which range in age from Middle Pennsylvanian (Lower Missourian Series) to Recent. The sediments consist primarily of marine limestones, calcareous shales, and sandstones. Minor amounts of siltstone and mudstones are also present. Neither igneous nor metamorphic rocks are exposed in the area, although Rejas (1965) mapped two small granitic exposures approximately two miles to the south.

A generalized stratigraphic column of the units mapped is given in Figure 4 and their areal distribution is shown on the geologic map (Plate 1). Cross-sections constructed through the mapped area are shown on Plate 2 with cross-section EE´ having the most complete stratigraphic sequence.

Because this investigation is primarily concerned with the upper member of the Moya Formation and its associated mineralization, only brief descriptions of the mapped units are given. For more detailed lithologic and paleontologic descriptions of these units the reader is referred to Rejas (1965, p. 11-46).

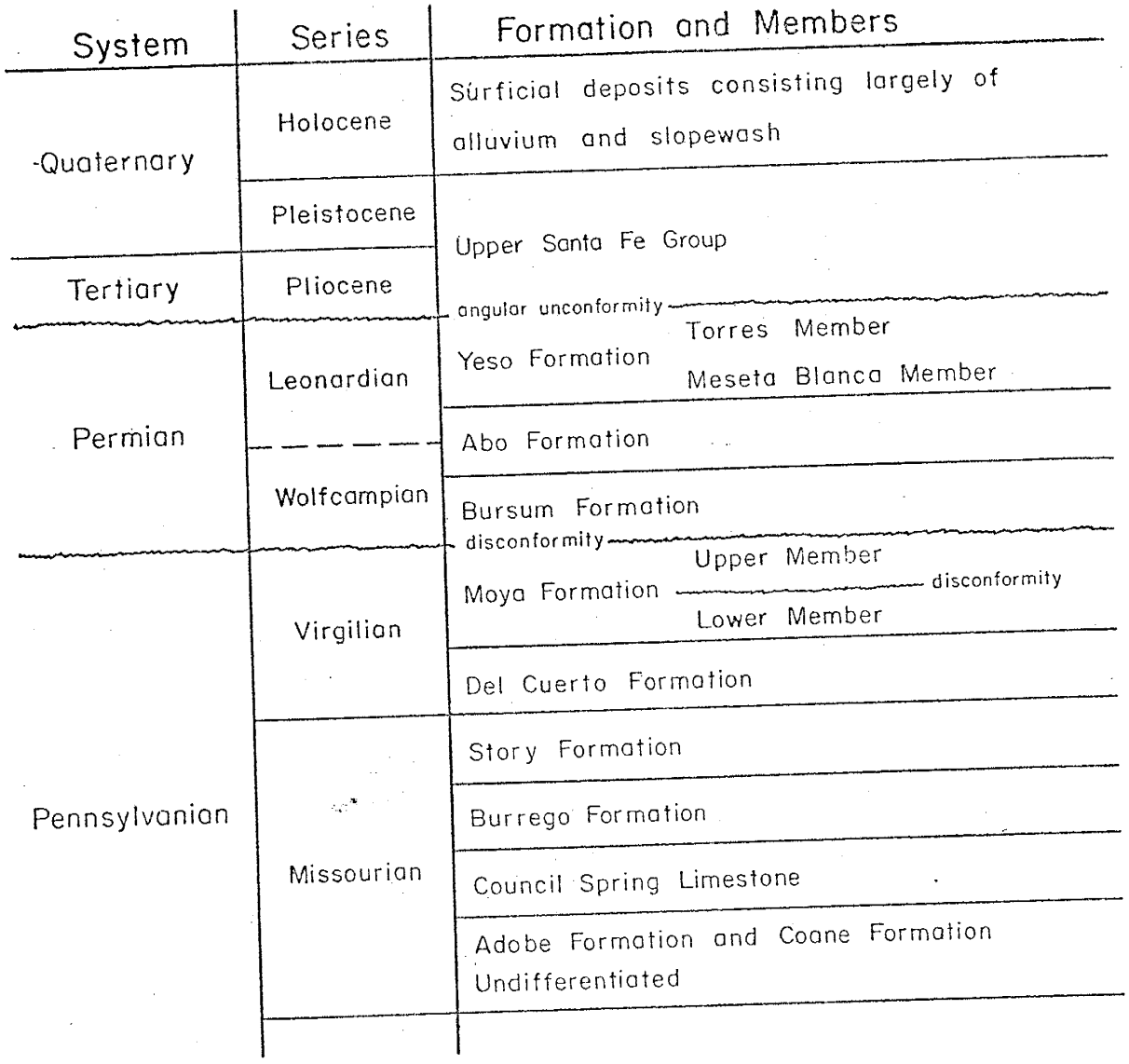

Figure 4. Generalized stratigraphic column of lithologic units exposed in the Chupadero Mines area.

Pennsylvanian System

Adobe Formation and Coane Formation (lower Missourian Series)

The oldest bedrock unit mapped in the Chupadero Mines area was the combined Adobe and Coane Formations, here defined as the Adobe-Coane undifferentiated. These two formations were mapped as a single unit because of their similar lithologies; interbedded limestones and shales. Because of the lithologic variation of the Adobe-Coane undifferentiated across the Amado fault zone, an eastern and a western section were described.

The western section of the Adobe-Coane undifferentiated is approximately 420 feet thick, as estimated from cross-section EE´ (Plate 2). Color of this section varies from light gray to orangish gray on both fresh and weathered surfaces (Figure 5). The stratigraphic section is composed of a basal sequence of medium-bedded limestones which become thinner and more shaley stratigraphically upward (Figure 5). The limestone beds consist of micrite, pelmicrite, dismicrite and biomicrite.

Thickness of the Adobe-Coane undifferentiated east of the Amado fault zone was not measured or estimated because of limited exposures; however, Rejas (1965) estimated a thickness of 258 feet. The eastern section consists

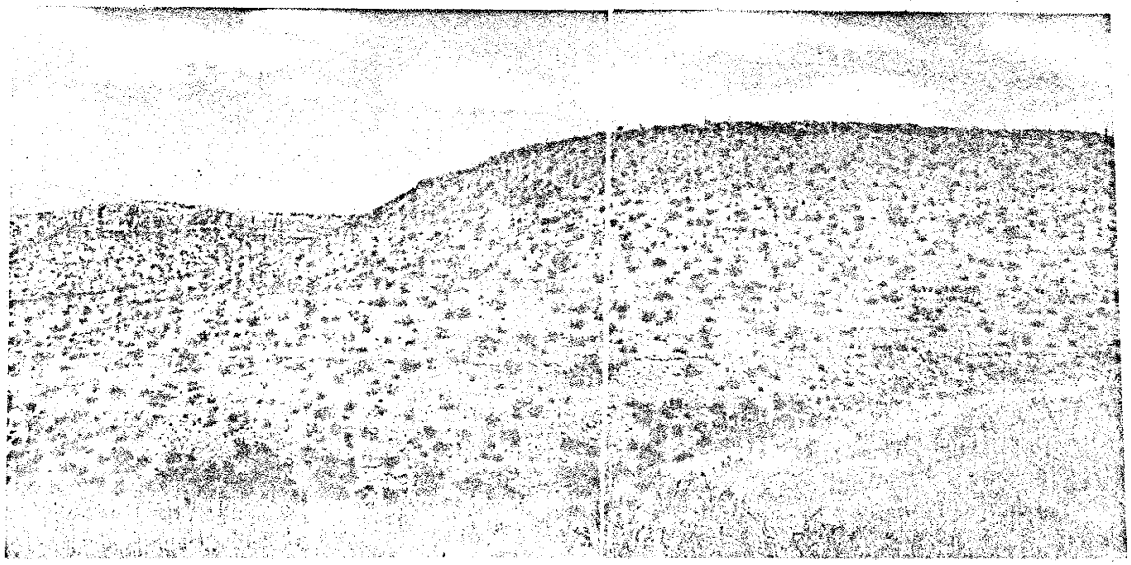

Figure 5. Upper portion of the Adobe Formation and Coane Formation, undifferentiated, capped by the Council Spring Limestone in southwest portion of study area. View to northwest. The orange-gray bands are medium-bedded limestones and the gray units are fissile shales. Hambleton (1959) identified a bioherm underlying the thicker, wedge-like mass of Council Spring Limestone near the left margin of photograph. The bioherm is located just outside the western margin of the study area.

predominately of calcareous, fissile shales interbedded with thin-bedded limestones. These individual rock units have colors similar to those of the western section. The micritic limestones are fossiliferous in the basal sequence and become less fossiliferous in the stratigraphically upward direction. A yellowish gray to greenish gray, massive-bedded and cross-bedded, arkosic sandstone occurs in the upper one third of the unit (Figure 6).

Council Spring Limestone (Middle Missourian Series)

The Council Spring Limestone is approximately 20 feet thick and conformably overlies the Adobe-Coane undifferentiated. Color of the Council Spring Limestone ranges from light gray to dark gray on both fresh and weathered surfaces. Where exposed, the unit forms prominent topographic features such as ledges and cliffs (Figures 5 and 6). The weathered surfaces of this formation are characterized by a distinct pit-and-cusp texture. The cusps bordering the edges of the irregularly-shaped pits have sharp edges.

As in the Adobe-Coane undifferentiated the lithology of the Council Spring Limestone varies laterally across the Amado fault zone. West of the Amado fault zone the

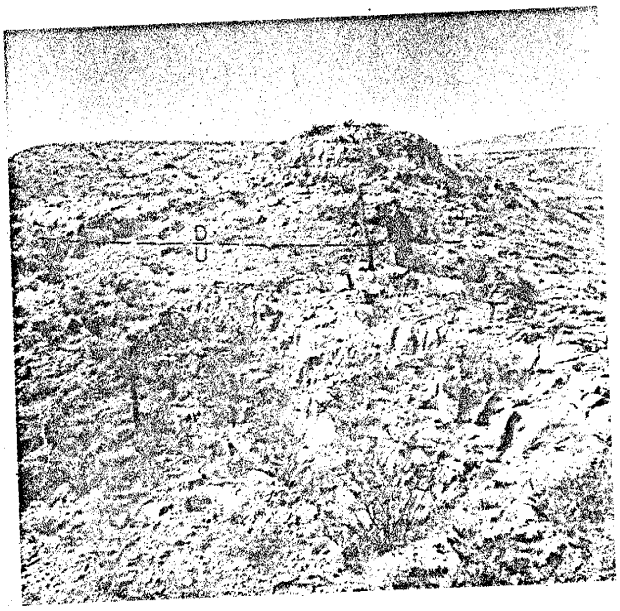

Figure 6. Upper portion of the Adobe-Coane, undifferentiated, and the Council Spring Limestone, east of the Amado fault. Resistant, light-colored rock unit in lower one-half of photograph is one of the prominent arkosic sandstones in the eastern section of the Adobe-Coane, undifferentiated. The small hillock behind the man is capped by a remnant of the Council Spring Limestone. This feature is separated from the arkosic sandstone by a bifurcation of the Amado fault (dashed line).

unit is composed entirely of fossiliferous micrite. East of the fault zone the unit consists of dismicrite and fossiliferous micrite with scattered stringers of dark-brown chert.

Burrego Formation (Middle Missourian Series)

The Burrego Formation conformably overlies the Council Spring Limestone. Exposures of the Burrego and younger bedrock units occur only west of the Amado Fault zone (Plate 1). Fresh surfaces of the formation range in color from light gray to medium gray with minor tones of yellowish-gray. Weathered exposures are predominately gray, with green and brown tones also present. The Burrego Formation is approximately 90 feet thick. The lower 35 feet of the formation consists of a basal calcareous shale which grades upward into a shaley, fossiliferous micrite. This sequence is overlain by a fine-grained, well-cemented, subarkosic sandstone approximately 10 feet thick. The upper 45 feet of the formation consists predominately of argillaceous, fossiliferous micrites, interbedded with calcareous shales and siltstones. The uppermost micrite unit becomes arenaceous near the contact with the overlying Story Formation.

Story Formation (Upper Missourian Series)

The Story Formation conformably overlies the Burrego Formation and varies in measured thickness from 20 feet in drill-hole 13 (Plate 1 and Appendix I) to approximately 50 feet in Section EE´ (Plate 2). The Story can be divided into two distinct lithofacies: a lower brownish-gray to reddish-purple clastic unit overlain by light-gray to brownish-gray limestones. The lower clastic unit is composed of very fine-to fine-grained, calcareous arkosic sandstones which grade upward into calcareous siltstones and micaceous shales. The overlying limestone unit consists of micrites and crinoidal biomicrites with thin interbeds of calcareous shale. Many of the crinoids have undergone silification and are more resistant to weathering than the surrounding host rock, hence they stand out in relief.

Del Cuerto Formation (Lower Virgilian Series)

The Del Cuerto Formation conformably overlies the Story Formation and ranges in measured thickness from 25 feet in drill-hole 13 (Plate 1 and Appendix I) to 55 feet in Section CC´ (Plate 2). Three distinct lithofacies were recognized within the formation, a yellowish-brown to reddish-purple lower and an upper clastic facies separated

by a light-gray limestone facies. The lower clastic facies consists of a basal shaley unit overlain by a calcareous, subarkosic sandstone. The subarkosic sandstone grades upward into the middle limestone facies composed of silty, fossiliferous micrites. Silicified crinoids within this unit, like those of the Story Formation, are resistant to weathering and stand out in relief. The upper clastic facies consists of a calcareous shale which grades upward into a fine-grained, micaceous, arkosic sandstone. Feldspars within this unit have altered to a white clay.

Moya Formation (Upper Virgilian Series)

The Moya Formation overlies the Del Cuerto Formation and is approximately 70 feet thick. Rejas (1965) divided the formation into a lower and an upper member based on their lithologic identities. This division has been followed in this investigation.

Lower Member

The lower member of the Moya conformably overlies the Del Cuerto Formation and ranges in thickness from 35 feet in drill-hole 13 (Plate 1 and Appendix I) to 50 feet in Section EE′ (Plate 2). Color of the member is light gray on both fresh and weathered surfaces although brownish gray or olive

gray may predominate locally. Like the majority of the thicker limestone units in the mapped area, the lower Moya forms conspicuous ledges and cliffs where exposed. Lithologically the unit consists of fossiliferous micrite and dismicrite which contain numerous stylolites. Where exposed, the upper and lower surfaces of the stylolites are covered by a clay-rich coating, characterized by greenish gray color.

Upper Member

The upper member of the Moya disconformably overlies the lower member of the Moya and ranges in measured thickness from 15 feet (Plate 2, Section EE´) to 35 feet in drill-hole 13 (Plate 1 and Appendix I). The upper Moya consists of a basal clastic sequence which is overlain by more resistant limestones. Because the copper mineralization in the Chupadero Mines area is localized in the basal clastic sequence, it was studied in detail both lithologically and paleoenvironmentally. During the examination of the upper Moya, the member was divided into three lithofacies: 1) sandstone, 2) siltstone-shale, and 3) limestone (Figure 7). Particular emphasis was placed on the sandstone lithofacies because the dominant mineralization is localized in this unit.

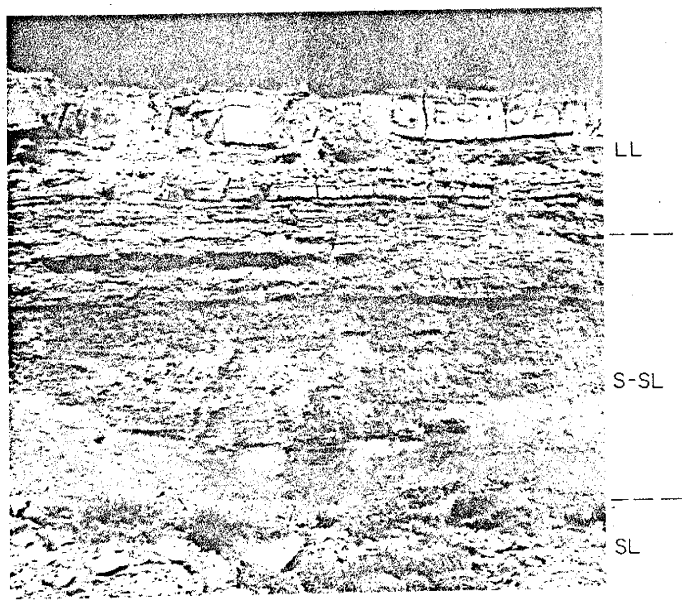

Figure 7. Exposure of the top two-thirds of the upper Moya along the western wall of the North Pit. Approximate contacts between the three lithofacies are dashed: SL=sandstone lithofacies, S-SL=siltstone-shale lithofacies, LL=limestone lithofacies.

Sandstone lithofacies

The sandstone lithofacies is usually the lowest stratigraphic unit of the upper Moya and where present, appears to disconformably overlie the lower member of the Moya Formation. The disconformity can be recognized in the central portion of the study area (Figure 8), but it could not be identified farther west where the basal bed of the upper Moya is an arkosic micrite (Figure 9). Geometry of the sandstone lithofacies is lenticular to pod-like in cross-section and varies in measured thickness from a minimum of two to three inches to a maximum of 21 feet in drill-hole 18 (Appendix I). Measured thicknesses of individual strata range from very thin-bedded to medium-bedded; in general, bed thicknesses decrease upward.

Primary structures identified in the sandstone lithofacies consists of cross-bedding, ripple marks, parting lineations, a slump structure (?), and a cut-and-fill structure (?). Cross-bedding was the only depositional structure recognized in the undisturbed bedrock and was used to estimate flow direction during the deposition of the sandstone lithofacies. Individual cross-strata rarely exceed one foot in thickness while the cross-bedded cosets seldom exceed a composite thickness greater than four feet

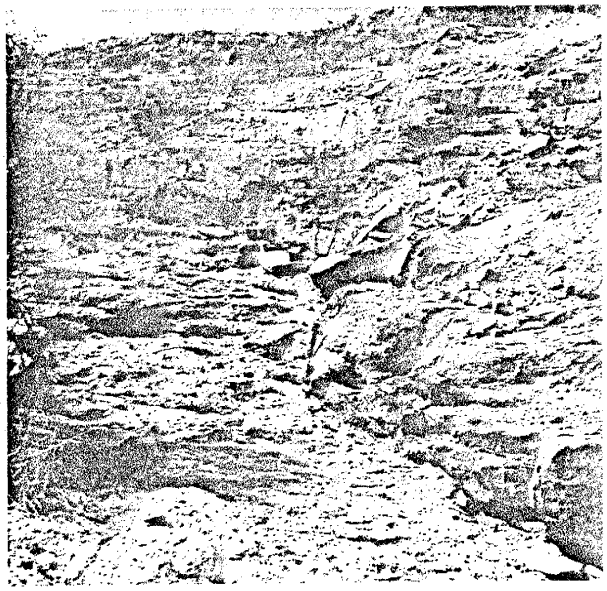

Figure 8. Contact between the upper and lower members of the Moya Formation approximately 50 feet north of the southern adit. View is to the southwest. The head of the hammer is resting on the disconformable contact separating the brownish, basal sandstone of the upper Moya from the light-gray, fossiliferous micrite of the lower Moya. Green color of rocks in the middle distance is malachite mineralization adjacent to portal of the southern adit. Prominent cliff in the distant background is the limestone unit of the up faulted Story Formation.

Figure 9. Contact between upper and lower members of the Moya Formation (dashed line) near western edge of study area. The disconformity noted between these two members in the central portion of the mapped area could not be identified at this location. The bedded, blocky material is an arkosic micrite, the lowest unit of the upper Moya at this site.

(Figure 10). The general east-west strike and dips from 25 to 35 degrees to the north of the cosets suggest that the approximate flow direction during the deposition of the sandstones was from the south to the north (Figure 10).

Asymmetrical ripple marks were identified in the disturbed material of the South Pit. Their wave lengths ranged from four to six inches while their amplitudes were approximately ½ to one inch. Parting lineations also occurred in the bulldozed rubble of the South Pit. These structures were localized in the fine-to medium-grained sandstones.

A feature similar in appearance to a slump structure (?) was identified near the portal of the northern adit (Plate 1 and Figure 11). The warped attitude of the siltstones and shales underlying this feature suggests either slumping or differential compaction. One possible cut-and-fill structure (?) was recognized in the medium-grained, sandstone near the portal of the southern adit (Figure 10) although no additional structures of this type were identified, possibly because of the limited number of exposures.

Fractures and joints in the sandstone lithofacies are numerous, especially along the fault which cuts the North Pit. Bedding-plane fractures are the most numerous and often occur along the carbonaceous shale partings

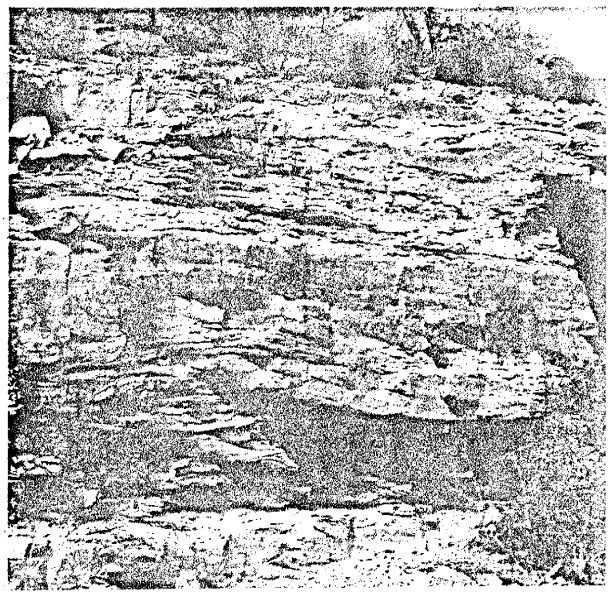

Figure 10. Structures in the sandstone lithofacies (arkosic and subarkosic arenites) of the upper Moya adjacent to the southern adit. View is west-northwest. The cross-strata of the lower beds dip approximately 25-35 degrees to the north. Thicknesses of individual cross-strata are less than one foot, with cosets not exceeding four feet. The relative flow direction during the deposition of the sandstones was from the south to the north (left to right in picture). A possible cut-and-fill structure can be seen truncating the cross-strata approximately three feet below and slightly to the left of the rock hammer. The light-green surficial staining in the upper one-third of the picture is malachite.

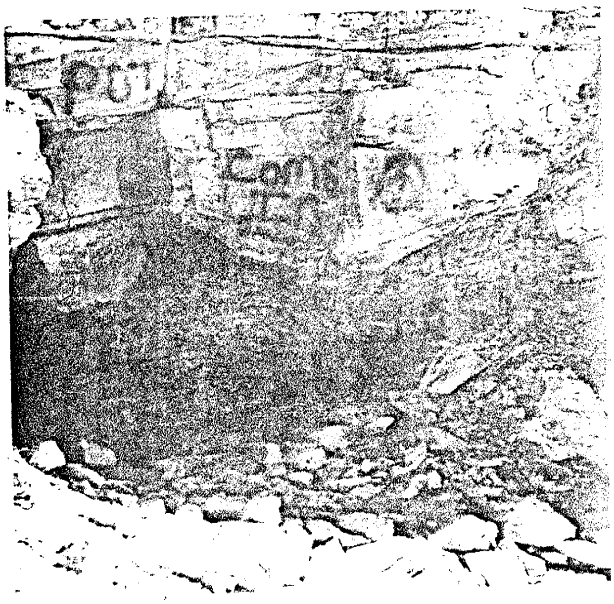

Figure 11. A slump structure or differential compaction feature in the upper Moya, at the portal of the northern adit. The structure can be seen approximately one foot above the handle of the rock hammer. Faint malachite mineralization occurs along the basal contact of the sandstone.

interbedded with the sandstones. The majority of these secondary structures have been filled by calcite, hematite, gypsum and minor quartz. The fractures or joints which are filled with gypsum are confined solely to the North Pit. Many of the fracture-fillings often exhibit cross-cutting relationships which suggest multiple stages of filling.

Lithologically, the sandstone lithofacies consists of grayish-orange to pale-moderate reddish brown, arkosic and subarkosic arenites and wackes which are often color banded and mottled (Figure 12). Composition of the sandstones were determined by petrographic analysis of 18 thin sections cut from drill-hole cores. The classification scheme used during the petrologic study is presented in Appendix II. In general, the sandstone lithofacies is characterized by a basal sequence of very coarse-to coarse-grained, arkosic and subarkosic arenites which grade stratigraphically upward into fine-to very fine-grained, arkosic and subarkosic wackes. The wackes are usually interbedded with thin laminations of carbonaceous shale near the contact with the overlying siltstone-shale lithofacies. Several large plant fragments (two to three inches in longest dimension) were observed in the bulldozed float of the South Pit. These fragments generally occurred along carbonaceous bedding-planes in the wackes and have been replaced by

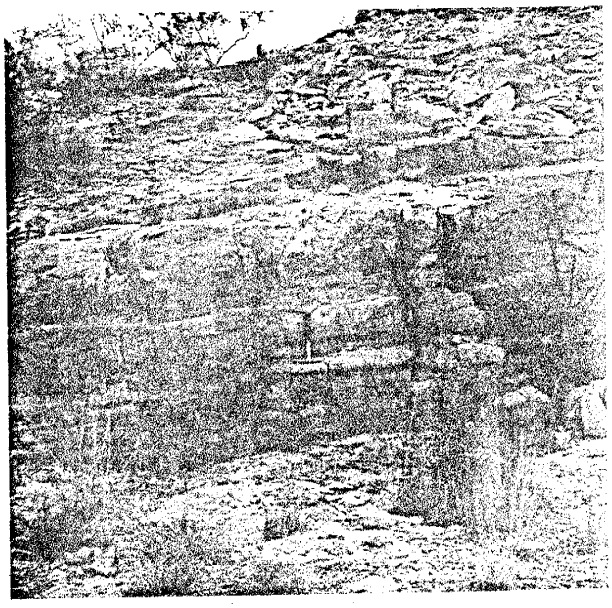

Figure 12. Colored banded and mottled basal sandstone (arkosic and subarkosic arenite and wacke) disconformably overlying the fossiliferous micrite of the lower Moya. View to north of the southern margin of the South Pit. Color banding is a function of iron oxide concentration. The mineralized rubble in the upper right-hand corner was bulldozed from the South Pit.

iron oxides. Iron oxide concretions observed in the sandstone lithofacies appeared to be most common in the fine-to medium-grained arkosic and subarkosic wackes.

The textural features of both the arenites and wackes observed in thin section are summarized in Table 1. In comparing the arenites to the wackes it is interesting to note that the textural features of the two groups are very similar, including the framework components used in the Folk's ternary classification scheme (Appendix II). The only component which varied greatly between the arenites and wackes was the percentage of matrix, which is to be expected. The matrix in the arenites and wackes appeared to be composed of finely-divided quartz and mica. Many times the matrix was obscured by both calcite and hematite cements. In general these cements usually averaged about 15 to 20 percent in the arenites and 10 to 15 percent in the wackes. Both hematite and calcite often appear to etch the quartz and feldspar grains. In some instances these two cements exhibited coincident relationships possibly indicating multiple stages of cementation. Minor amounts of quartz also occur as interstitial cement.

Other detrital grains noted in thin section were hematite, muscovite and fibrous plant remains. Hematite

ARENITES	
Average percentage of classification components	quartz 74%, feldspar 25%, rock frags. 1% matrix 11%
Grain size	varies from very coarse (2.0mm) to very fine (.065mm)
Grain shape (roundness)	angular to subrounded
Surface texture	pitted and corroded
Grain contacts	tangential to straight most common
Replacement	hematite and calcite replacing quartz, feldspar; iron oxides replacing woody fragments; feldspars altering to clays
WACKES	
Average percentage of classification components	quartz 74%, feldspar 25%, rock frags. 1% matrix 33%
Grain size	varies from medium (.5mm) to very fine (.065mm)
Grain shape (roundness)	angular to subangular
Surface texture	pitted and corroded
Grain contacts	floating to tangential most common
Replacement	calcite and hematite replacing quartz and feldspar, iron oxides replacing woody fragments

Table 1. Textural features of the arkosic and subarkosic arenites and wackes of the upper Moya sandstone lithofacies.

usually occurred as discrete grains of fine-grain size (.125mm) which were characterized by dark, blood-red centers with lighter reddish-orange halos. Thin crusts of hematite coat some quartz and feldspar grains. Books of muscovite are oriented parallel to the bedding but are generally contorted into irregular shapes around detrital grains probably because of compaction. Minor amounts of fibrous plant detritus occurred in several of the fine-grained, arkosic and subarkosic wackes. The plant fragments, like the books of mica, were usually oriented parallel to bedding and had undergone deformation similar to that of the mica books. Iron oxide halos generally surrounded the plant detritus.

In considering the overall textural variations of the sandstone lithofacies, the sediments change markedly upward. Generally grain size decreases and sorting becomes poorer. The percentage of matrix increases while cement decreases and grain shape (roundness) becomes more angular.

Siltstone-shale lithofacies

The siltstones and shales of the upper Moya have been combined into a single unit (siltstone-shale lithofacies) because of their complex vertical and lateral character. This lithofacies, generally the middle unit of the upper

Moya, is characterized by gradational and interbedded contacts with the underlying sandstone lithofacies and the overlying limestone lithofacies (Appendix I, and Figure 7). Geometry of the siltstone-shale lithofacies is very irregular, ranging from lenticular to sheet-like. Measured thicknesses of the unit vary from paper-thin partings along bedding-planes to a maximum of 14 feet in drill-hole 17 (Appendix I).

Although the siltstones and shales were combined into a single lithofacies, both lithologies are described individually to avoid confusion.

The siltstones of the upper Moya are calcareous, micaceous and sandy, and are characterized by a moderate-yellowish brown to a grayish-orange color on both fresh and weathered surfaces. Thicknesses of the siltstone strata range from laminated to very thin-bedded. Bedding-plane surfaces are often undulatory. Primary structures in the siltstones consist of several small areas of possible bioturbation; secondary structures occur as fractures or joints. Many of these structures have been filled by hematite, sparry calcite and sometimes gypsum. Those fractures or joints containing gypsum are restricted to the west wall of the North Pit (Plate 1).

The siltstones are coarse grained (.062 to .031mm) and

are composed predominately of quartz with minor amounts of feldspar and finely-divided mica. Many of the quartz and feldspar grains appear to have been etched by both calcite and hematite cements. Relic, cubic ghosts of possible pyrite were also observed in the siltstones but have since been oxidized to hematite or limonite. Minor amounts of detrital plant and shell debris were identified in the siltstone lithofacies. The plant detritus which is generally associated with carbonaceous shale partings has been replaced by iron oxides. Brachiopod and mollusk shell debris is commonly found in pockets near the contact with the overlying limestone lithofacies, and has undergone neomorphic recrystallization.

The shales of the siltstone-shale lithofacies are carbonaceous, micaceous and fissile-bedded, and range in color from medium-dark gray to light brown on both fresh and weathered surfaces. No primary structures were identified, although stringers and veinlets of gypsum possibly related to fractures or joints are common in the shales of the west wall of the North Pit (Plate 1 and Figure 13).

Authigenic pyrite, 1 to 2mm in size, is ubiquitous throughout the shale beds, and much has been oxidized to hematite and limonite. Plant detritus in the shales has

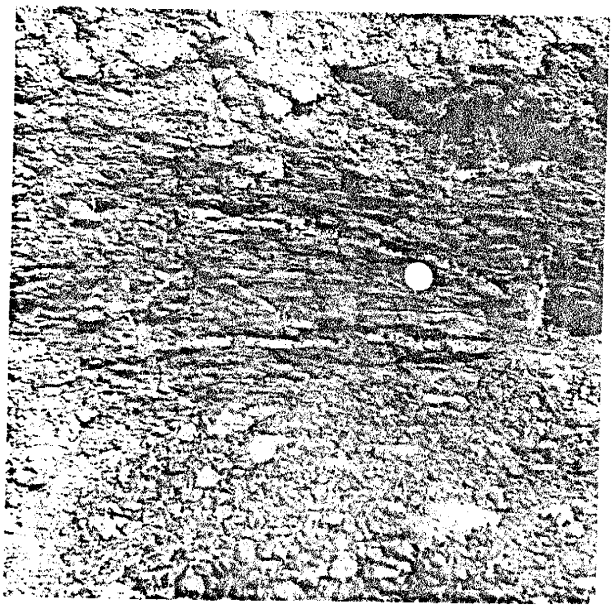

Figure 13. Close-up view of gypsum veinlets containing malachite and azurite and cross-cutting the carbonaceous shale of the upper Moya, six to eight feet to the right of center of Figure 7.

commonly been replaced by both hematite and limonite.

Iron oxide concretions are commonly found in the shales of the upper Moya. Their sizes vary from ½ to 3 inches in greatest dimension and their shapes are globular to ellipsoidal (Figure 14). Some of the concretions are composed of framboidal pyrite and are surrounded by iron-oxide halos. Colors of the concretions vary from dark reddish-brown to brassy-metallic yellow.

Limestone lithofacies

The limestone lithofacies, the top unit of the upper Moya, has a gradational contact with the underlying siltstone and shale lithofacies but is thought to be separated from the overlying Bursum Formation by a disconformity (Rejas, 1965). Geometry of this lithofacies is undulatory and sheet-like with measured thicknesses ranging from a minimum of five feet in drill-hole 13 to a maximum of 18 feet in drill-hole 3 (Appendix I and Plates 1, 3, 4, and 5). Bed thicknesses in this unit range from very thin to very thick and generally increase upwards (Figure 7). No primary sedimentary structures were identified in this lithofacies, although fractures or joints oriented at various angles with no apparent directional preferences are common. Many of these secondary structures have been filled by sparry

Figure 14. Close-up view of the carbonaceous shale of the upper Moya, six to eight feet left of center of Figure 7. Note rust-colored, iron-oxide concretions within the carbonaceous shales. Both the shale and the concretions have been cross-cut by fibrous gypsum veinlets.

calcite or siderite.

Lithologically, the limestone lithofacies consists of a basal yellowish-brown, silty to arenaceous, nodular micrite which grades upward into brownish-gray biomicrites. Clastic constituents in the basal unit are composed of quartz, feldspar, and minor amounts of mica and hematite (limonite). Feldspars have altered to clays while much of the detrital material has been etched by both calcite and siderite. Grain size of the clastic material ranges from very fine to coarse, and grain shape (roundness) varies from angular to subangular. The biomicrites have a calcilutite texture in which grain size is less than 1/16mm. Some zones of the biomicrites have undergone porphyroid neomorphism, and the majority of the fossil fragments have a neomorphic, diagenetic texture. Fossil fragments in the biomicrites consist of brachiopod shells and spines, crinoid stems, mollusk shells and bryozoan detritus. All of these fragments are considered to be allochthonous because of their fragmental condition.

Chert concretions are scattered throughout the limestone. Several of the concretions appear to be replacing concentrations of fossil fragments. The cherts weather dark gray in contrast to the lighter hues of the limestones.

Environmental interpretation of the sandstone lithofacies of the upper Moya

In order to establish the depositional environment of the mineralized host rock, the sandstone lithofacies of the upper Moya, six sedimentary environments were studied to determine which model or models best fitted the observed features. The environments considered were: barrier bar, chenier plain, delta (distributary channel), fluvial (alluvial), lagoon (restricted), and tidal flat (intertidal zone). The "material process and response model" of Krumbein and Sloss (1963, p. 252) was used as a guideline. Additional information was obtained from Conybeare and Crook (1968) and Pettijohn, Potter and Siever (1972).

Table 2 lists the observed features of the upper Moya sandstone lithofacies and compares them to characteristics associated with each of the six sedimentary environments. The sedimentary model or models having the largest number of fractures in common with the sandstone lithofacies was selected as representing the probable environment of deposition. Table 2 indicates that the fluvial (alluvial) model and the delta (distributary channel) model are the most likely depositional environments. The barrier bar, chenier plain, lagoon, and tidal flat models are excluded

Table 2

Comparison of observed features of the upper Moya sandstone lithofacies with features common to barrier bars, chenier planes, delta (distributary channels), fluvial (alluvial), lagoons (restricted), and tidal flats (intertidal zone).

* C=common to environment: * R=rare to environment: * Blank space=features are not characteristic of the particular environment.

	Barrier bar	Chenier plain	Delta (distributary channel)	Fluvial (Alluvial)	Lagoon (restricted)	Tidal flat (intertidal zone)
GEOMETRY						
Length-undeterminable						
Width-undeterminable						
Thickness-min. of inches to a max. of 21 ft.	C	R	C	C		
External Geometry-lenticular to pod-like lenses	C	C	C	C	C	
Bifurcating	R	R	C	C		
SEDIMENTARY PROPERTIES						
Clastics						
grain size-very fine (.062mm) to very coarse (2.0mm) sand	C	C	C			
grain shape (roundness)-angular to subrounded	R		C	C	C	C
surface texture-pitting and minor frosting	C		C	C		
sorting-poor to moderate			C	C	R	C
composition-arkosic and subarkosic arenites and wackes			C	C		C
Nonclastics						
organics-minor amounts of fibrous plant remains		C	C	C	C	C
cements-calcite, hematite, quartz and (gypsum)	C	C	C	C	C	C
oxidation of sediments-color banding and mottling			C	C		
SEDIMENTARY STRUCTURES						
Inorganic structures (primary)						
cross-bedding-25-35 dip (1 ft. thickness of cross-strata) (unidirectional)			C	C		
ripple marks-(asymmetrical) small amplitude and wave length	R		C	C		C
parting lineations	R		C	C		C
slump structures			C	C		
cut-and-fill structures			C	C		
bed thickness (1-6 inches to 1-2 ft.)	C	C	C	C		C
disconformable basal contact	R		C	C		
Organic structures						
worm burrows		R	C	R	C	C
Chemical structures (secondary)						
concretions-iron-oxide (hematite)			C	C	C	
AREAL VARIATIONS						
Vertical decrease in grain size (fining upward)			C	C		
Lateral tapering and gradation of sandbodies into siltstone and shale lithofacies	C		C	C	C	

because of the low number of features in common with the sandstone lithofacies (represented by the large number of blank spots in Table 2). Additional features of the four environments which were not observed in sandstone lithofacies but which substantiate the above conclusion are listed below.

1) Barrier bar-conformable basal contact, large scale cross-bedding, concentrations of shell detritus (lag deposits) and heavy minerals, general coarsening upward of grain size.

2) Chenier plains-conformable basal contact, lag deposits, well-developed soil horizon and upward increase in grain size.

3) Lagoon (restricted)-abundance of silt and clay size material, argillaceous lime muds and possible evaporites.

4) Tidal flat (intertidal zone)-sheet-like geometry, lag deposits, flaser bedding, multidirectional cross-bedding and upward increase in grain size.

The fluvial (alluvial) and delta (distributary channel) environments, are genetically similar and have nearly identical features.

A typical fluvial environment, a fine-to coarse-grained channel, is flanked by natural levees and flood plain deposits. Channel geometry is very elongate, with channel patterns varying from meandering to bifurcating. Deposits of this type are usually lenticular to pod-like in cross-section and range in thickness from several inches at the flanks of these deposits to more than 100 feet. Structures associated with fluvial deposits include cross-bedding, asymmetrical

ripple marks, parting lineations, deformational features (slump or compaction structures) and scouring. There is usually an excellent correlation between the internal directional structures and the elongation of the channel body (Pettijohn et. al., 1972). Sedimentary properties associated with clastic sediments of the fluvial model (size, roundness, sphericity, surface texture, composition and sorting) have a high degree of variability. Petrographically, these sediments range from immature to mature and they are further characterized by varying amounts of detrital and chemical cements (Pettijohn et. al., 1972). Minor amounts of carbonaceous debris are commonly associated with these deposits. Areal variations of the fluvial environment are quite distinct; the basal contact is disconformable and the grain size decreases upward to multistory sandbodies (Allen, 1965). Lateral variations include intertonguing of the channel facies with the flood plain or overbank deposits forming serrate edges.

Delta distributary channels are one of the many subenvironments which form part of a deltaic complex. In general, all of the features commonly associated with a typical fluvial environment also are found in the distributary environment, except for certain relationships observed in bar finger sands. Bates (1953) described this relationship by

noting that bar finger sands are deposited at the mouths of distributary channels which flow into standing bodies of water. These deposits are distinctively elongate and form the framework of the delta. Features associated with these deposits include multidirectional cross-bedding, lag deposits, and an upward increase in grain size. The multidirectional cross-bedding is generally found in the lower portion of the sandstone sequence and is a function of wave and current action from the open marine shelf. One feature which is common in the distributary channels and bar finger sands but not the fluvial environment is bioturbation (worm burrows). Worm burrows are normally associated with brackish to marine waters and not fresh water.

Since the structures and features of both the fluvial environment and the distributary channel environment (excluding bar finger sands) are very similar to those of the upper Moya, either of these two environments could have been the setting for the deposition of the upper Moya sandstone lithofacies. In comparing the observed lateral facies changes of the upper Moya in the Chupadero Mines area, drawn diagrammatically below, evidence favors the distributary channel environment.

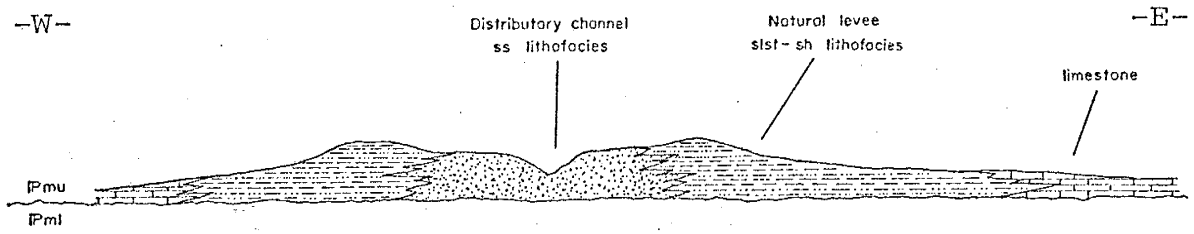

The sandstone lithofacies probably represents deposition in a channel facies with the coarser grained arenites deposited at the base of a point bar sequence, grading upward into the finer grained arenites and wackes. The siltstone-shale lithofacies appears to represent natural levee or overbank deposits, while the limestones occurring at the flanks of the clastic sediments probably were deposited in the shallow marine environment of a restricted bay. The intertonguing between the various facies shown in the diagrammatic cross-section suggests lateral migration of the channel complex. The strikes and dips from cross-bedding in the sandstone lithofacies suggest that granitic source rocks to the south and possibly southeast of the Chupadero Mines area were topographic highs during upper Virgilian time.

Permian System

Bursum Formation (Wolfcampian Series)

The Bursum Formation overlies the Moya Formation and has been assigned to the Lower Permian by Wilpolt et. al. (1946). Rejas (1965) suggested a disconformity exists between the Moya and the Bursum. Thickness of the Bursum estimated from cross-section EE´ is approximately 200 feet, although only 100 feet was logged in drill-hole 13 (Plate 1

and Appendix I). The discrepancy in thickness can be explained by a probable fault between the depths of 198 to 231 feet. This interpretation was made by Marshall Reiter (1972, personal communication) who conducted a thermal well-log test in drill-hole 13 and found a thermal anomaly between the depths of 198 to 231 feet, and according to him this suggests a fault. Vertical movement along this fault could account for the abrupt thinning of the unit at this drill-hole site.

The Bursum consists predominately of a series of reddish-gray mudstones and siltstones with interbeds of gray shale. A quartz-pebble conglomerate and several thin, nodular weathering limestones interbedded with gray, fissile shales occur in the lower two-thirds of the formation. Generally, the youngest unit of the Bursum Formation is a very coarse-grained, arkosic sandstone although it may be locally overlain by a thinly-laminated, gray shale approximately three feet thick (Figure 15). Both the quartz-pebble conglomerate and the very coarse-grained, arkosic sandstone contain conspicuous grains of pink orthoclase which range from 1mm to 1cm in greatest dimension. Subangular to subrounded clasts (½ to 4cm) derived from Pennsylvanian limestones and arkoses also were noted within

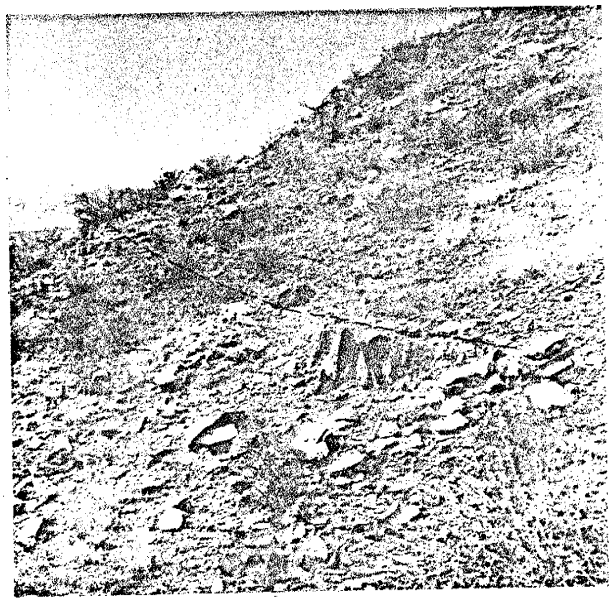

Figure 15. Conformable contact (dashed line) separating the thicker bedded and jointed, grayish, arkosic sandstone of the Bursum Formation from the overlying reddish-brown, laminated sandstone-siltstone of the Abo Formation.

the coarser-grained clastic units of the formation.

Abo Formation (Wolfcampian to Leonardian Series)

The Abo Formation conformably overlies the Bursum Formation and is approximately 330 feet thick. For the purpose of this investigation the contact between these two formations was placed above the stratigraphically highest gray shale or grayish, arkosic sandstone of the Bursum and below a laminated, fine-grained sandstone-siltstone of the Abo (Figure 15). The Abo has a very conspicuous pale-reddish brown color on both fresh and weathered surfaces.

Lithologically, the formation is largely calcareous shales and mudstones, with lesser interbedded siltstones, and fine-grained, feldspathic sandstones. The majority of the clastic units are laminated to very thin-bedded and often exhibit undulatory, mudcracked or ripple marked bedding-plane surfaces. Several thin limestone pebble conglomerates occur in the basal portion of the Abo Formation.

Yeso Formation (Leonardian Series)

Needham and Bates (1943) recognized four members within

the Yeso Formation. The four members listed in ascending order are: Meseta Blanca Sandstone, Torres Member, Cañas Gypsum and Joyita Sandstone. Only the two lower members crop out in the mapped area.

Meseta Blanca Sandstone Member (Leonardian Series)

The Meseta Blanca Sandstone Member conformably overlies the Abo Formation in the northeast corner of the mapped area and is approximately 300 feet thick. The contact separating these two formations was placed between a laminated, pale-reddish brown, sandy siltstone of the Abo and a cross-bedded, grayish-pink, feldspathic sandstone of the Meseta Blanca (Figure 16).

The Meseta Blanca Member consists largely of pale-red to grayish-pink, feldspathic and arkosic sandstones with interbeds of light-gray siltstone and shale. The sandstones are well-sorted and very fine- to fine-grained and are often cross-bedded.

Torres Member (Leonardian Series)

The Torres Member conformably overlies the Meseta Blanca Sandstone Member and is confined to several small remnants in the northeast corner of the study area (Plate 1).

Figure 16. Conformable contact (dashed line) between the Abo Formation and the overlying Meseta Blanca Sandstone Member of the Yeso Formation. Uppermost unit of the Abo is a pale-reddish brown, laminated and fine-grained, sandstone-siltstone and the basal unit of the Meseta Blanca is a grayish-pink, cross-bedded arkose.

Maximum thickness of these remnants as estimated from cross-sections AA′ (Plate 2) was 20 feet. The contact between the two members was placed between the light-gray, basal limestone bed of the Torres and the underlying pale reddish brown, fine-grained arkose of the Meseta Blanca. The Torres Member consists of massive to thick-bedded dismicrite and argillaceous micrite.

Tertiary-Quaternary Systems

Upper Santa Fe Group (Pliocene to Pleistocene)

Isolated remnants of the Upper Santa Fe Group are found capping the rolling hills in the northwest corner of the mapped area. These local deposits rest with angular unconformity upon the Abo Formation and they appear to thicken to the northwest. A maximum thickness of approximately 35 feet for these deposits was estimated from surface exposures. The Upper Santa Fe Group consists largely of pale-red conglomerates interbedded with fine-to medium-grained sandstones. Much of the fragmental material within this unit has been derived from nearby Pennsylvanian and Permian strata; limestones, mudstones and arkosic sandstones. Locally, this material has been cemented by caliche.

Quaternary Slope Wash

Slope wash deposits consist of poorly-sorted deposits of angular to subangular rock fragments, sand and silt. These materials have accumulated in topographic lows and near the base of slopes.

Quaternary Alluvium

Alluvium deposits consist of angular to subangular, poorly-sorted accumulations of rock fragments, sand and silt. These deposits are found within the intermittent stream courses which dissect the mapped area.

STRUCTURE

The major structural features in the Chupadero Mines area and in the surrounding region consist of complexly faulted Pennsylvanian and Permian bedrock. Faults in this region are generally high-angle, normal faults which have very complicated and irregular trends. The dominant faulting in the Chupadero Mines area occurs in the south-central portion and is very complex because of bifurcating, hinging and cross-cutting relationships. A conspicuous feature associated with many of the faults is a creamy-white, coarse, crystalline calcite which occupies the fault planes and breccia zones (Figure 17). Individual bodies of this type of calcite are vein-like and range from several inches to as much as five feet in width. Slickensides identified within several of these calcite zones suggest secondary movement along some faults.

Faults in the Chupadero Mines area can be grouped into two classifications: 1) high-angle, normal faults and 2) low-angle, thrust sheets. Of the numerous high-angle, normal faults mapped in the study area, three major faults were identified. The first major fault (Fault 1, Plate 1) occurs in the central portion of the mapped area and bisects the North Pit. This fault has a general northeast trend

Figure 17. Fault surface exposed in arroyo wall near center of study area (dashed line indicates fault plane). Jointed limestone of lower Moya on left has moved down with respect to the massive limestone of the Del Cuerto Formation. A coarse-crystalline calcite vein occupies the fault zone, left of hammer.

and has a maximum displacement of approximately 650 feet near the northern boundary of the mapped area. Drag folding, as well as strike-slip movement may be associated with Fault 1. Evidence which supports the drag-fold hypothesis is based on the abundance of bedding-plane fractures which were observed in the upper Moya sandstone lithofacies adjacent to Fault 1 in the North Pit. Strike-slip movement is suggested by the lack of copper mineralization in drill-hole 13 east of the North Pit and also east of Fault 1.

The second major fault (Amado fault, Plate 1) is located in the southeast corner of the mapped area. This fault is characterized by a general northeast trend and numerous bifurcations which parallel its strike (Plate 1). The Amado fault appears to be hinged to the south-southwest and has a maximum displacement of 450 feet along the eastern margin of the study area. Like Fault 1, the Amado fault may also have associated strike-slip movement. This conclusion is based on the abrupt lateral facies change of the Adobe Formation and Coane Formation, undifferentiated, across the fault. Both the Amado fault and Fault 1 form the eastern and western margins, respectively, of the northeast-trending graben in the Chupadero Mines area.

The third major fault (Fault 3, Plate 1) has a general

northwest to north-south strike and divides the study area into nearly equal halves. Maximum displacement along this fault is approximately 165 feet. Fault 3 appears to be the southwestern boundary for the northeast-trending graben in the mapped area (Plate 1).

Numerous other high-angle, normal faults were mapped, but they are not as pronounced as the three major faults previously described. Generally, these minor faults have strikes which are parallel and subparallel to the major faults and displacements ranging from a minimum of two to three feet to a maximum of approximately 100 feet.

Remnants of two low-angle thrust sheets were identified in the study area (Plate 1). Both features are limited in areal extent and quite thin. At the northern thrust sheet, both the thrust sheet and the underlying bedrock consist of a silty sandstone of the Meseta Blanca Sandstone Member, hence this feature was identified only because of the exposed slickensides and fault surfaces. The direction of movement of this thrust sheet is from south to north (Plate 1). The southern thrust sheet consists of the fossiliferous micrite of the Del Cuerto Formation which has overridden the arkosic sandstone of the upper Moya. Direction of relative movement here is thought to have been from north to south (Plate 1).

Folding in the mapped area is minor except for a zone

of intense deformation in the southwest corner (Plate 1). Here fold axes have a southeast trend and plunge moderately to the northwest. This zone is confined stratigraphically to the Adobe-Coane Formations, undifferentiated (Plate 1, and Figure 18). In general, most folds appear to be asymmetric with minor thickening and thinning of individual beds. Movement has occurred along some bedding-planes as indicated by the presence of slickensides.

Because fault systems could not be clearly distinguished in the Chupadero Mines area, the relative ages of structural deformation could not be determined in the study area. The structural relationships and the ages of structural deformation were observed by Rejas (1965) in the Cerros de Amado area and surrounding regions. Listed below in probable chronological age (from oldest to youngest) are the deformational structures (fault systems and folds) which were recognized by Rejas (1965).

1) Fault system number 1 includes high-angle, normal faults which trend approximately N. 40° E. These faults affect rocks only of Pennsylvanian and Permian age and are dated as post-Permian and middle (?) Miocene to Pleistocene.

2) A zone of intense deformation (folding) which has a general northwest trend affects rocks only of Pennsylvanian age in the Cerros de Amado area but is dated post-Permian and post-fault system number 1. Although this appears to be an ambiguous age date, it is verified by the lack of offset where the Amado fault intersects this zone of intense deformation.

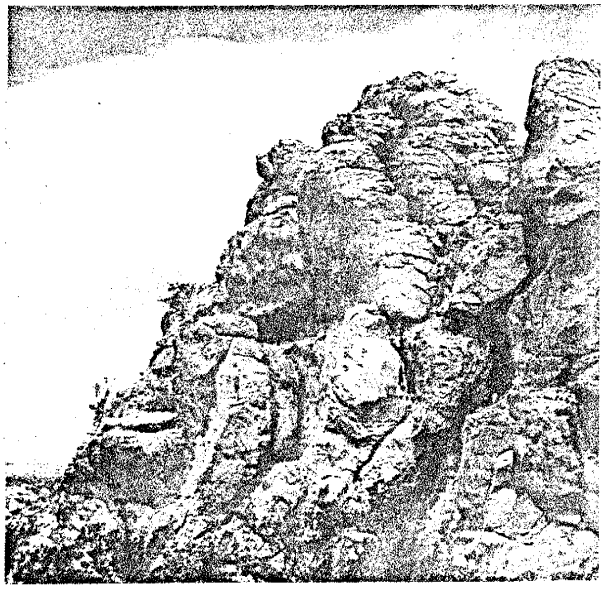

Figure 18. Folded limestone remnant of the Adobe-Coane, undifferentiated, in extreme southwest corner of mapped area. View to north. The rock hammer is located near the fold axis which trends southeast and plunges to the northwest. Note local thickening and thinning of beds. Eroded portion of the unit has apparently overturned.

3) Fault system number 2 includes high-angle, normal faults which trend approximately north-south. These faults affect rocks as young as the Datil Group (early (?) Miocene) but are covered by the Santa Fe Group (middle (?) Miocene to Pleistocene). Therefore the age of this fault system is dated as early (?) Miocene and pre-middle (?) Miocene to Pleistocene.

4) Fault system number 3 is a set of high-angle, normal faults which strike approximately north-south. These faults offset the Santa Fe Group and are dated as early (?) Pleistocene in age.

In comparing the observed structures mapped during this investigation (Plate 1) with those described by Rejas (1965), some similarities are noted. The major Faults 1 and 2 have general northeast trends and affect only Pennsylvanian and Permian strata and therefore, they may be grouped into Fault system number 1 recognized by Rejas (1965). The major Fault 3 has a general north-south trend and as it affects only Pennsylvanian and Permian strata in the study area, it may belong to either Fault systems number 2 or 3 of Rejas (1965). The zone of intense deformation in the southwest corner of the study area can be correlated with that mapped by Rejas (1965) and therefore has the same age of structural deformation. Multiple stages of movement along many faults, evidenced by offsets, bifurcations and cross-cutting relationships (Plate 1) did not allow more concise interpretation of the deformational ages.

ECONOMIC GEOLOGY

Copper mineralization observed at the Chupadero Mines area is confined stratigraphically to the upper member of the Moya Formation (Plate 1). Most of the mineralization is localized in the sandstone lithofacies, with minor amounts in the siltstone-shale lithofacies (Appendix I and Plates 3,4 and 5).

Six copper minerals were identified in the study area and they are listed below in order of decreasing abundance:

1) malachite $Cu_2CO_3(OH)_2$
2) azurite $Cu_3(CO_3)_2(OH)_2$
3) tenorite CuO
4) cuprite Cu_2O
5) delafossite $CuFeO_2$
6) chrysocolla $CuSiO_3 \cdot 2H_2O$

These minerals occur as: 1) interstitial cements, 2) fracture-fillings, 3) concretions, and 4) replacements of fibrous plant remains (numbers 3 and 4 are illustrated in Figure 19).

Copper Mineralization in the Sandstone Lithofacies

The distribution of copper mineralization in the sandstone lithofacies is irregular and discontinuous. In

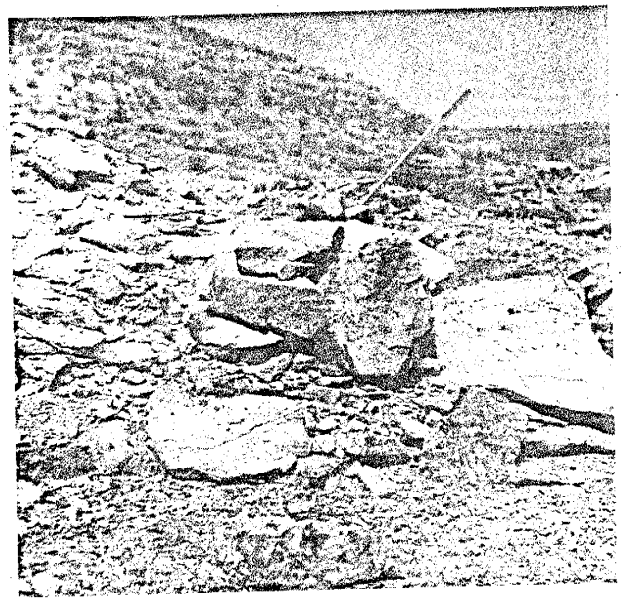

Figure 19. Bulldozed rubble from South Pit with three tabular blocks of mineralized upper Moya sandstone in the center of photograph. The lowest, nearly horizontal fragment shows a fracture surface coated with malachite. The overlying block contains a delafossite concretion surrounded by a concentric halo of malachite and azurite. The vertical block to the right shows two plant fragments that have been replaced by malachite and iron oxides.

general, the mineralization appears to be localized in the fine-to medium-grained arkosic and subarkosic arenites and wackes with only minor amounts identified in the very coarse-to coarse-grained arenites (Appendix I and Plates 3, 4 and 5). Malachite and azurite are by far the two most abundant copper minerals in the sandstone lithofacies. Both of these copper carbonates are commonly associated with calcite and hematite and generally occur as interstitial cements and fracture-fillings. Occurrences were observed where malachite and azurite cements appear to have etched quartz and feldspar grains, although previous calcite or hematite cements may have originally done the etching and have since been replaced. Minerals which occur as interstitial cements often exhibit coincident or overlapping depositional relationships. In some exposures malachite and azurite cross-cut hematite and calcite while in other exposures the reverse genetic sequence is observed.

Stringers of malachite and azurite not related to fractures, but parallel to the bedding, are common. These dendritic veinlets weave in and around detrital grains and sometimes terminate abruptly. Detrital books of mica oriented parallel to the bedding are commonly stained by these copper carbonate veinlets.

Fractures and joints in the study area containing copper mineralization are restricted to the areas in and around the two open pits, particularly the North Pit. Bedding-plane fractures are the most numerous of these secondary structures and have been filled primarily by malachite, azurite, hematite and calcite in varying proportions. The malachite which occurs as fracture-fillings is commonly enveloped by thin, discontinuous crusts of tenorite. Gypsum veinlets and stringers containing botryoidal masses and veinlets of the copper carbonates also fill several of these secondary structures. Fracture-filling minerals, like those of the interstitial cements, often exhibit cross-cutting relationships which suggest coincident or overlapping depositional patterns.

Three copper-bearing concretions were found in the loose, bulldozed rubble of the South Pit (Plate 1 and Figure 19). Two of these concretions are very distinct because of their black, opaque centers which are enveloped by concentric halos of malachite and azurite. Small irregularily distributed patches of hematite occur within these copper carbonate halos. Benner (1972, personal communication) x-rayed a similar concretion from the South Pit and found the black, opaque mineral in the center of the concretion to be delafossite ($CuFeO_2$). Although, the

opaque centers of the two concretions described previously were not x-rayed, their hardness of 5.5 and color and streak (both black) suggest the mineral to be delafossite.

The other concretion found in the South Pit was very dense and somewhat irregular in geometry. A surficial coating covering the periphery of the concretion consisted of malachite, tenorite and minor amounts of hematite. The concretion was cut in half revealing a mottled interior of intergrown cuprite, tenorite and malachite.

Minor amounts of fibrous plant detritus, in the fine- to medium-grained arkosic and subarkosic arenites and wackes have been replaced by malachite and hematite (Figure 19). These fragments are most numerous along carbonaceous shale partings which occur near the contact with the overlying siltstone-shale lithofacies.

Copper Mineralization in the Siltstone-Shale Lithofacies

Copper mineralization in this lithofacies consists of malachite and azurite which occur as isolated botryoidal masses along the fissile-bedded shales and as fracture-fillings (Figure 13). The copper carbonates which occurs as fracture-fillings are commonly associated with gypsum and fill fractures both oblique and parallel to bedding. No copper-bearing concretions or replacement of fibrous plant

detritus were observed in this unit. In general, mineralization is restricted to within three to five feet both above and below a sandstone contact.

Suggested Copper and Iron Stability Fields and Their Applications to Paragenesis

The compositions of malachite, azurite, tenorite, cuprite, delafossite and hematite (limonite) may be defined by the components Cu, Fe, O_2, CO_2, and H_2O. Stability relations among these minerals and other oxides and carbonates of copper and iron can be conveniently shown using partial pressure diagrams (cf. Garrels and Christ, 1965). Under earth surface conditions, (25°C, 1 atmosphere) the activity of H_2O in dilute solutions is very nearly = 1. By writing reactions conserving copper and iron between solid phases, stability relations among minerals observed at the Chupadero Mines may thus be represented in terms of fugacities of CO_2 and O_2. The values of equilibrium constants for such reactions are calculated using tabulated standard free-energy values of appropriate species listed in Table 3. Although equilibrium constraints are strictly written in terms of fugacities of gas species, the fugacity may be equated to partial pressure at 25°C and 1 atmosphere. At one atmosphere total pressure, the partial pressures of O_2 and CO_2 may not exceed unity.

Native Copper	Cu	0.00 a
Tenorite	CuO	-30.50 c
Cuprite	Cu_2O	-34.98 a
Delafossite	$CuFeO_2$	-111.90 d -114.70 b
Malachite	$Cu_2CO_3(OH)_2$	-216.44 a
Azurite	$Cu_3(CO_3)_2(OH)_2$	-343.73 c
Siderite	$FeCO_3$	-161.06 a
Hematite	Fe_2O_3	-177.10 a
Magnetite	Fe_3O_4	-242.40 a
Water (liquid)	H_2O	-56.69 a
Carbon dioxide (gas)	CO_2	-94.26 a
Oxygen (gas)	O_2	0.00 a

Table 3: Standard free-energy values (in kilocalories) used in calculations to construct partial pressure (fugacity) diagrams: a) Garrels and Christ (1965), b) Rossini et. al. (1969), c) Robie and Walbaum (1968), and d) Calculated from the equation $\Delta G = a + bT$ (Zalazinskii et. al. , 1969) for the reaction $\frac{1}{2}Cu_2O + \frac{1}{2}Fe_2O_3 = CuFeO_2$.

If ubiquitous water is involved, the partial pressure of oxygen is further restricted to the range $10^{-83.1}$ to 10^{0} according to the reaction limiting the stability of water; ie.

$$H_2O = H_2 + \tfrac{1}{2}O_2$$

Figures 20 and 21 illustrate stability relations among copper and iron compounds in the systems $Cu-O_2-CO_2-H_2O$ and $Fe-O_2-CO_2-H_2O$, respectively. Figure 22 is a composite diagram in which the iron stability fields of Figure 21 are superimposed on the copper stability fields of Figure 20. This composite diagram does not consider the possible chemical interactions between the two systems but merely permits comparison of assemblages occurring in each system.

The mineral delafossite ($CuFeO_2$) shown in Figure 23 serves to link both the copper and iron stability relations in the system $Cu-Fe-O_2-CO_2-H_2O$. In calculating the stability field for delafossite two different free-energy values were used (Table 3). The larger of the two delafossite fields (solid lines) was determined from a free-energy value equal -114.7kcal listed by Rossini et. al. (1969) while the smaller field (dashed lines) corresponds to a free-energy value equal -111.9kcal calculated from Zalazinskii et. al. (1969). By comparing Figures 22 to 23 it is evident that the mineral delafossite is stable over a relatively wide range of f_{O_2}

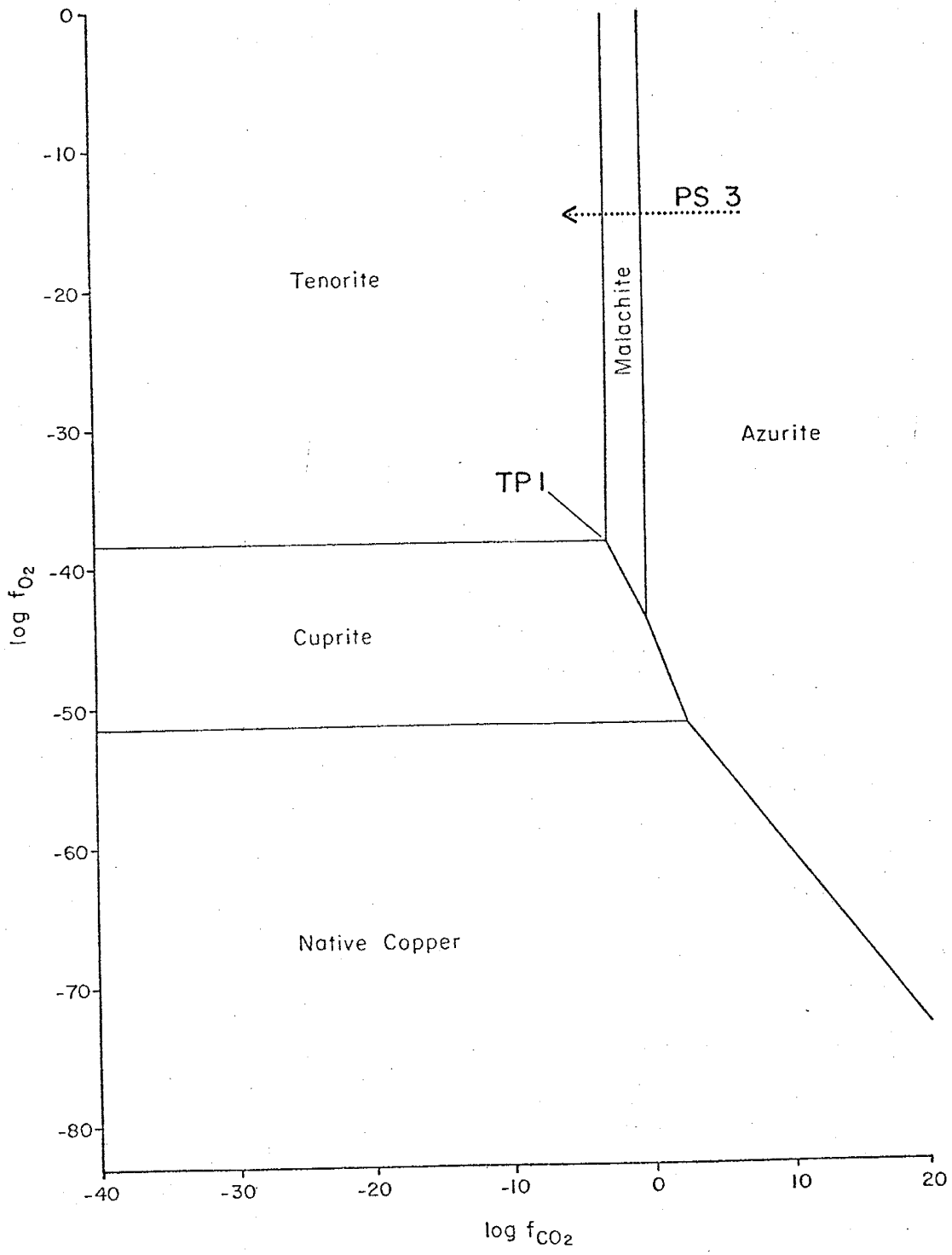

Figure 20. Stability of copper compounds as a function of fO_2 and fCO_2 at 25° C and 1 atm., pure liquid H_2O ubiquitous (Garrels and Christ 1965, p. 156)

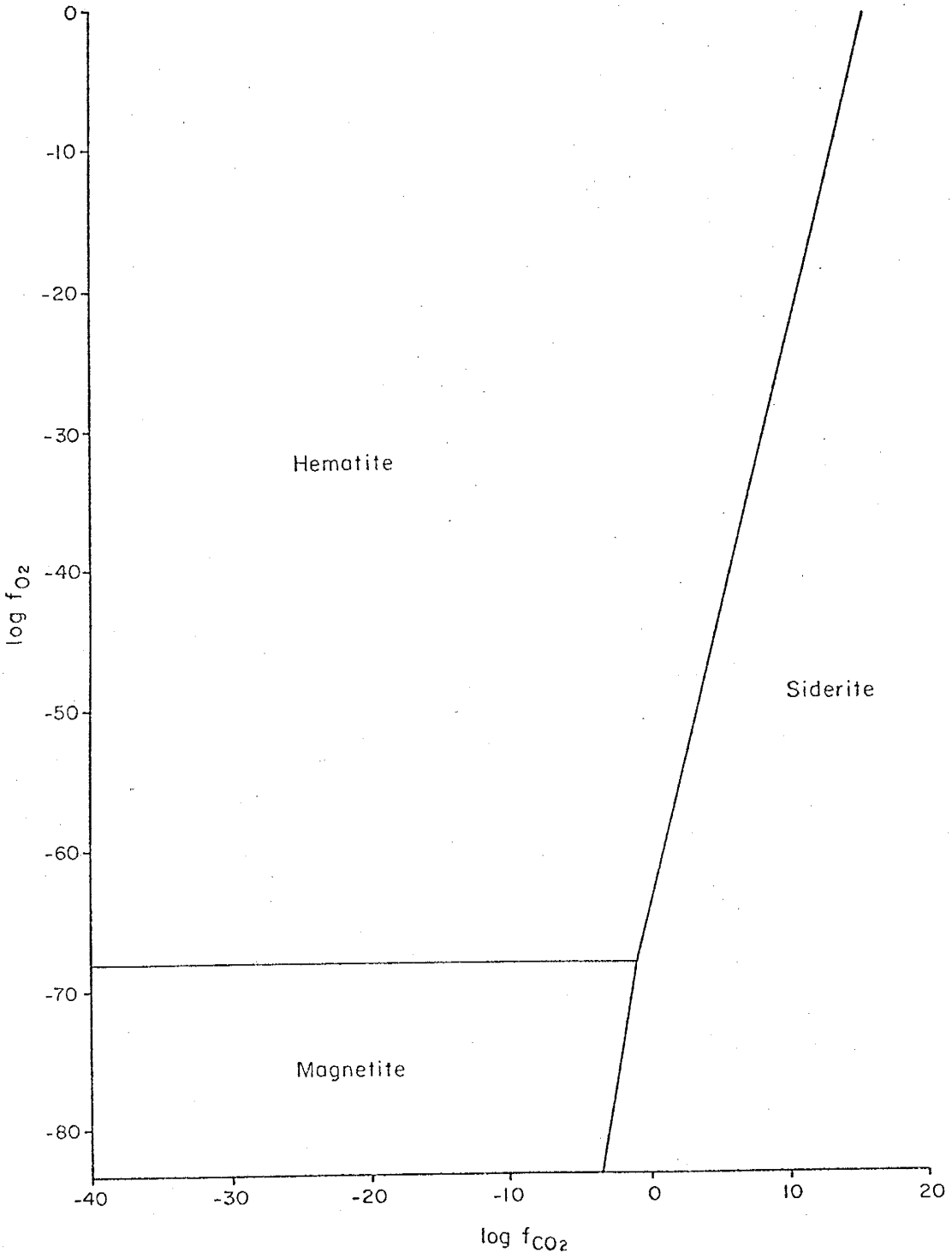

Figure 21. Stability of iron compounds as a function of fO_2 and fCO_2 at 25° C and 1 atm., pure liquid water ubiquitous (Garrels and Christ, 1965, p. 153)

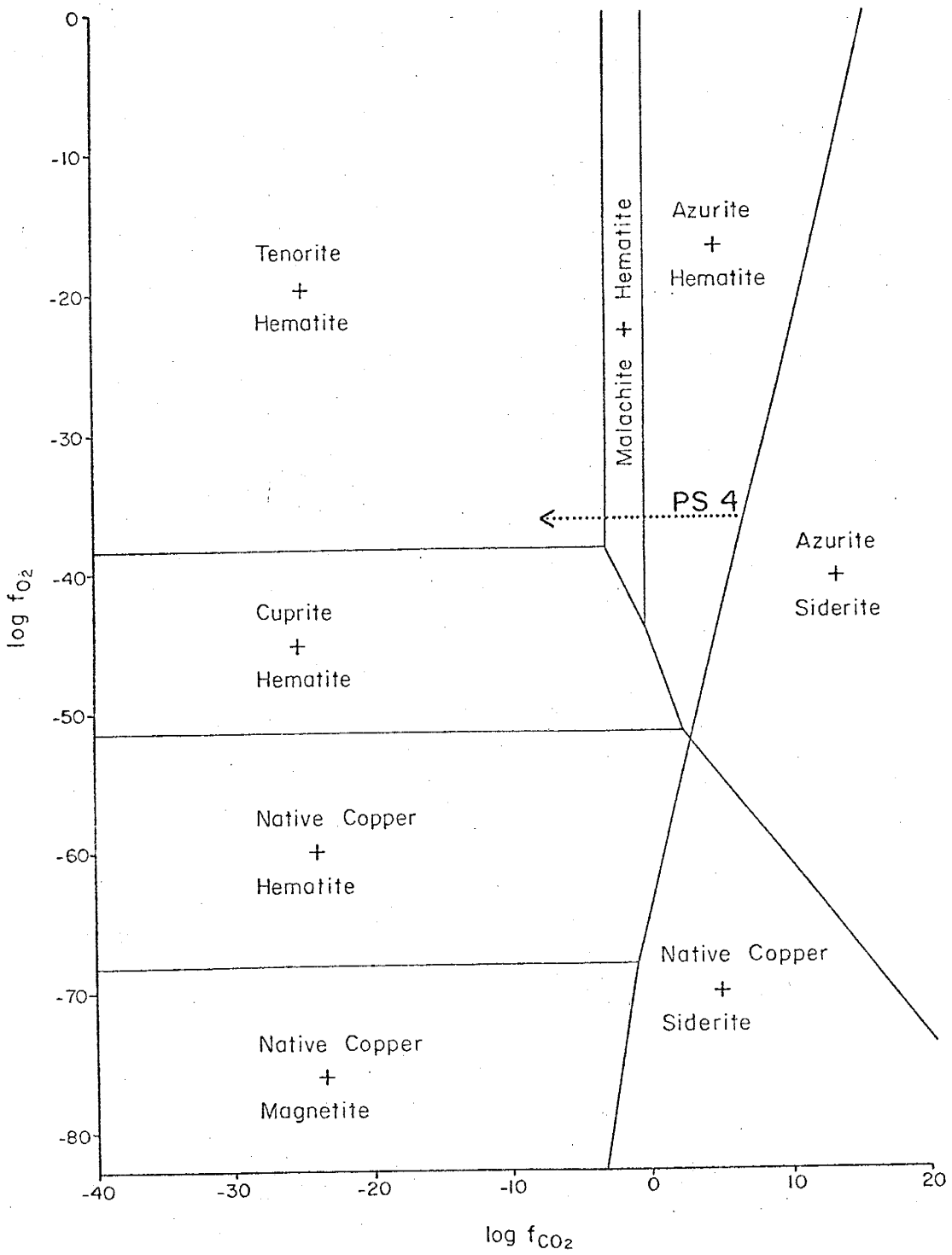

Figure 22. Stability of iron compounds (Figure 21) superimposed on copper compounds (Figure 20) as a function of fO_2 and fCO_2 at 25° C and 1 atm., H_2O ubiquitous.

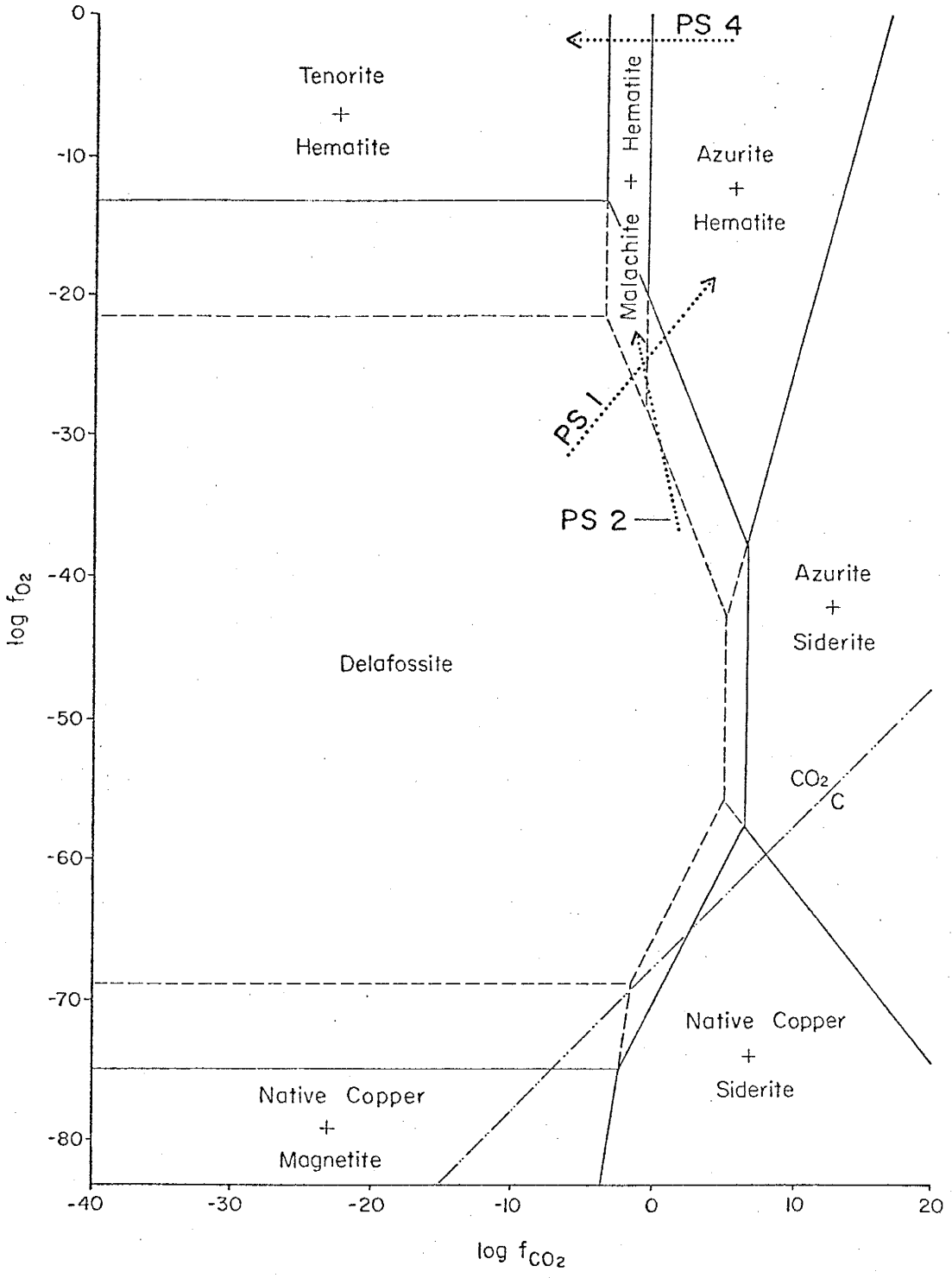

Figure 23. Stability relations among some iron and copper oxides and carbonates as a function of fO_2 and fCO_2 at 25° C and 1 atms, H_2O ubiquitous. ----Zalazinskii et. al. (1969), delafossite, —— Rossini et. al. (1969) data for delafossite.

and f_{CO_2} values. Delafossite replaces the entire cuprite + hematite field as well as portions of the surrounding stability fields shown in Figure 22.

The C-CO_2 equilibrium relation in the system CO_2-O_2 was superimposed on Figures 23,24 and 25 to show the relations between the two delafossite fields and that of carbon (C). The comparison between these stability fields brings out an interesting relationship in that the delafossite stability field as determined from data by Rossini et. al. (1969) coincides with that of carbon only in a very narrow range of f_{O_2} and f_{CO_2} values. This coincidence does not appear for the delafossite stability field calculated from data of Zalazinskii et. al. (1969).

Figures 24 and 25 were constructed by superimposing Figure 22 on each of the individual delafossite stability fields shown in Figure 23. These diagrams are overlain to show the possible mineral assemblages permitted at equilibrium. Of particular interest in this study are those minerals which coexist with delafossite. In comparing Figure 24 to 25 one difference is evident: that is, the presence of the delafossite $\pm$ (native copper or magnetite) stability field in Figure 24 which is absent in Figure 25. If the delafossite + magnetite mineral assemblage had been observed in the study area it would suggest that the larger of the two delafossite

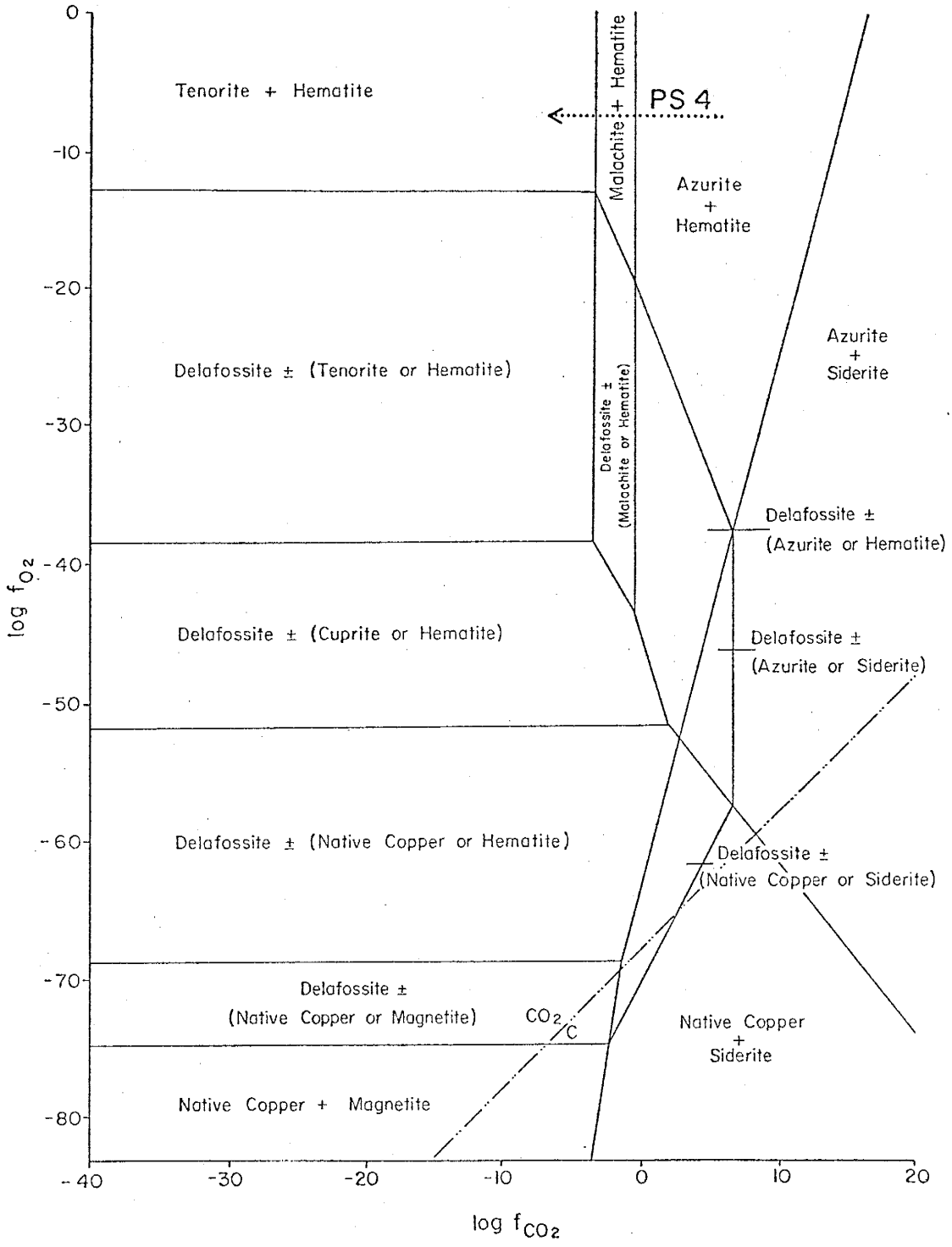

Figure 24. Stability field of delafossite determined from data by Rossini et. al. (1969) and Table 3, overlain by Figure 22 to show possible mineral combinations.

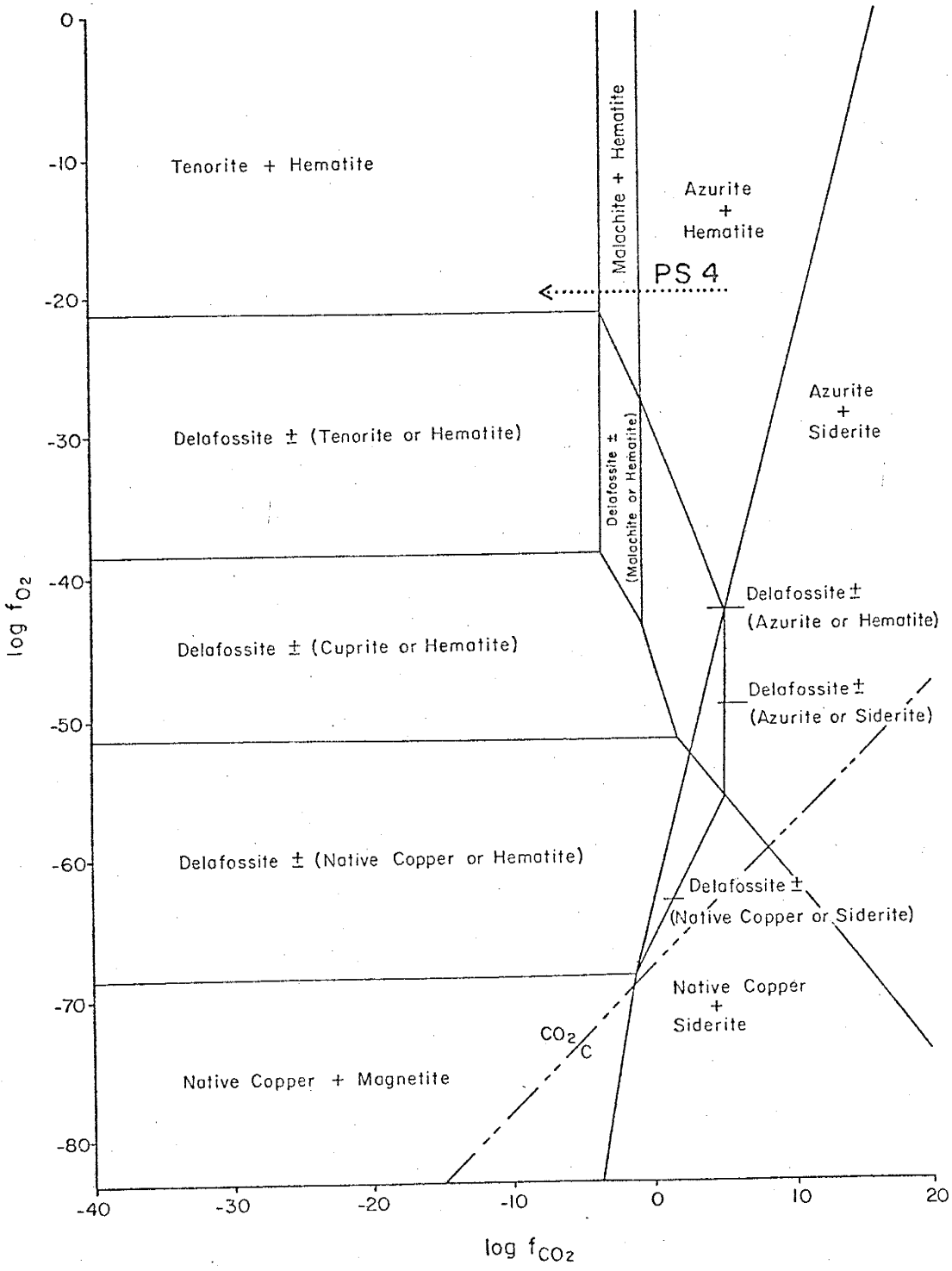

Figure 25. Stability field of delafossite determined from data by Zalazinskii et. al. (1969) and Table 3, overlain by Figure 22 to show possible mineral combinations.

stability fields (Figure 24), constructed from a free-energy value determined by Rossini et. al. (1969) in Table 3, is probably more correct. But because neither native copper nor magnetite were identified at the Chupadero Mines area it cannot be determined which of the two free-energy values is more accurate.

Examination of relative masses of coexisting minerals may provide an indicator of the amount of copper present in the system compared to that of iron. The procedure suggested for determining whether an environment contains excess iron or copper may be illustrated by the reaction:

$$Cu_2O + Fe_2O_3 \longrightarrow 2CuFeO_2$$

At 25° C and one atmosphere, with log f_{O_2} and log f_{CO_2} values restricted to the delafossite ± (cuprite or hematite) stability fields in Figures 24 and 25, the mineral reaction has three possible product assemblages:

1) if the amount of cuprite equals that of hematite, then the reaction will only form delafossite, with no excess of either of the two reactants:
$$Cu_2O + Fe_2O_3 \longrightarrow 2CuFeO_2$$

2) if the amount of cuprite is greater than that of hematite, then the reaction will form delafossite until all the hematite is consumed and the excess cuprite will then coexist with delafossite:
$$(1 + x)Cu_2O + Fe_2O_3 \longrightarrow 2CuFeO_2 + xCu_2O$$
Where x = the amount of excess cuprite above that which is needed to form delafossite with all available hematite.

3) if the amount of cuprite is less than that of hematite, then delafossite will form until all the cuprite is consumed and the excess hematite will coexist with delafossite:

$$Cu_2O + (1 + x)Fe_2O_3 \longrightarrow 2CuFeO_2 + xFe_2O_3$$

Where x = the amount of excess hematite above that which is needed to form delafossite with all available cuprite.

The three solutions described above not only hold for this particular reaction but for all phase assemblages containing delafossite and a possible coexisting iron or copper mineral as shown in Figures 24 and 25. The possibility does exist that selective leaching by later solutions could modify the observed product phases shown in Figures 24 and 25, although oxide minerals generally have a low solubility at near neutral pH typical of ground water environments, and, therefore, they probably would not be affected.

A comparison of the mineral stability fields shown in the six fugacity diagrams with the mineral assemblages observed in the Chupadero Mines area aided in interpretation of mineral paragenesis and genesis. The three copper concretions found in the South Pit offered the best mineral relationships for comparison to these six diagrams.

The two delafossite concretions surrounded by concentric halos of malachite and azurite, and containing minor amounts of hematite scattered within both copper carbonate halos, suggest copper to iron ratios greater than one. Because both the malachite + hematite and azurite + hematite

mineral assemblages are in contact with the delafossite, two paragenetic sequence are possible: 1) delafossite ⟶ malachite + hematite ⟶ azurite + hematite, and 2) delafossite ⟶ azurite + hematite ⟶ malachite + hematite. Both of these possible reaction paths are plotted on Figure 23 as dotted lines. The first paragenetic sequence (PS 1) suggests that copper reacted with iron to form delafossite at log f_{O_2} and log f_{CO_2} values restricted to those within the delafossite stability fields of Figure 23. As the iron was consumed during the formation of delafossite, excess Cu remained; and with increasing log f_{O_2} and f_{CO_2} values, the deposition of malachite + hematite was followed by azurite + hematite. The second paragenetic sequence (PS 2) suggests that delafossite formed under the same set of conditions as PS 1. The formation of azurite + hematite ⟶ malachite + hematite as indicated by PS 2 requires an increase in log f_{O_2} and a slight decrease in log f_{CO_2}, with excess copper present.

The other copper-bearing concretion found in the South Pit consists of cuprite, tenorite and malachite which are intergrown. Minor amounts of a discontinuous, surficial hematite stain were identified on the periphery of this concretion. The absence of any iron minerals intergrown with the copper minerals suggests that the two mineral assemblages

(copper and iron) were deposited at different time intervals. The intergrown and mottled texture of the three copper minerals suggests the formation of these at or about the same time. In comparing the mineral assemblage cuprite + tenorite + malachite to Figure 20, the indication is that all three minerals can coexist at a triple, or invariant, point (TP 1, at log f_{O_2} + -38.0 and log f_{CO_2} = -3.5) and were probably deposited simultaneously.

Other mineral relationships identified in the Chupadero Mines area, as fracture-fillings and as interstitial cements, are not as clearly defined as those observed in the copper-bearing concretions from the South Pit. Malachite and azurite with minor tenorite are the dominant copper minerals which occur as fracture-fillings and interstitial cements. These copper minerals are commonly associated with hematite and calcite and to a lesser degree gypsum.

Occurrences were observed where malachite halos azurite and where tenorite appears to envelope malachite. These mineral relationships suggest the following paragenetic sequence: azurite ⟶ malachite ⟶ tenorite. This sequence which is plotted on Figure 20 as PS 3, suggests initially high copper concentrations and relatively high f_{CO_2} values for the deposition of azurite. As the f_{CO_2} decreased, with either a decrease or an increase in f_{O_2}, the formation of

malachite, then tenorite proceeded. Because hematite is commonly associated with these minerals a similar paragenetic sequence (PS 4) consisting of: azurite + hematite ⟶ malachite + hematite ⟶ tenorite + hematite can be plotted on Figures 23, 24 and 25. The same f_{CO_2} and f_{O_2} constraints which probably governed the PS 3 paragenetic sequence are valid for the PS 4 paragenetic sequence.

Mineral Genesis

In collecting and comparing the evidence for the mineral genesis at the Chupadero Mines area, three modes of origin merit consideration: 1) fault control which acted as a plumbing system for ascending copper-bearing ground water solutions, 2) mineralization deposited by ground water moving laterally through a permeable sandstone, and 3) oxidation and leaching of a cupriferous shale by downward percolating meteoric waters.

Fault Control

Faulting must be considered as a possible control for the emplacement of the copper mineralization because both the North and the South Pits are bounded by faults (Plate 1). Copper-bearing ground waters may have moved upward along the

breccia zones of the faults and deposited the mineralization in the permeable sandstone lithofacies of the upper Moya. The possibility of chemical interaction between the ground waters and the interstitial cements of the somewhat permeable sandstone lithofacies may have been the factor which localized copper mineralization. The acidic ground waters carrying copper in solution (as Cu^{++}) may have reacted with the calcite cements freeing CO_2 gas which then reacted with the copper in solution and deposited both malachite and azurite.

Several observations noted in the field, however, contradict this hypothesis. First, the lack of mineralization associated with the fault breccia zone near the North and South Pits suggests that mineralization is probably not related to faulting. The absence of mineralization in the arkosic sandstone of the Del Cuerto Formation near the fault penetrated by drill-hole 12 (Plate 1), further negates any relationship of faulting to mineralization. Although the arkosic sandstone of the Del Cuerto Formation is lithologically similar to the upper Moya sandstone lithofacies, no mineralization was identified in that unit. The absence of mineralization in any of the sandstone units penetrated by drill-hole 13, east of the fault which bounds the North Pit (Plate 1 and

Appendix 1) also tends to disprove this hypothesis. The possibility of strike-slip movement along this particular fault must be considered and could explain why mineralization was not found in drill-hole 13.

The age of faulting in the Chupadero Mines area, as suggested from field observations, is pre-mineralization and post-lithification of the upper Moya sandstone lithofacies. The pre-mineralization age is based on the field evidence previously discussed while the post-lithification age requires additional information to substantiate this conclusion.

Many of the fractures and joints in and around the North and South Pits have been filled with copper mineralization suggesting that faulting is pre-mineralization and post-lithification. Although much of the copper mineralization occurs as interstitial cements, which possibly suggests a pre-lithification age, the abundance of replacement and enveloping relationships of hematite and calcite by malachite and azurite favor post-lithification. Another factor which challenges this hypothesis is the unknown origin for the copper-bearing ground waters.

Deposition by Ground Water

The second hypothesis suggests that copper minerals

were deposited by ground water moving laterally through a permeable zone, particularly sandstones. These ground waters could have reacted in a reducing environment produced by the carbonaceous material of the sandstone and siltstone-shale lithofacies, depositing primary chalcocite or delafossite. At a somewhat later time the primary mineralization could have been oxidized and leached forming the irregular stratabound deposit. Localization of mineralization in the permeable sandstone lithofacies of the upper Moya suggests a possible relationship between the copper deposit at Chupadero Mines and this mode of origin.

One of the major weaknesses of this hypothesis is the absence of observed chalcocite (Cu_2S) or any copper sulfide in the study area, although minor amounts of delafossite ($CuFeO_2$) were identified as concretions in the South Pit.

In this particular hypothesis a reducing environment in the sandstone lithofacies is a primary requirement for the formation of the chalcocite or delafossite. Although a reducing environment must have been present in the siltstone-shale lithofacies of the upper Moya, based on the abundance of organic detritus and ubiquitous pyrite, only minor amounts of organic detritus were identified in the sandstone lithofacies. In general, the organic material is localized in the fine-to medium-grained arenites and wackes

of the sandstone lithofacies near the contact with the overlying siltstone-shale lithofacies. The two delafossite concretions found in the South Pit occurred in relatively clean sandstones and were relatively free from any associated organic material, suggesting that delafossite may not have been deposited in a reducing environment and that the presence of organic matter had little influence on its formation.

Another feature which opposes the lateral ground water transport hypothesis is the lack of mineralization in the upper Moya sandstone where penetrated by drill-hole 13, east of the fault which bisects the North Pit (Plate 1 and Appendix 1). The sandstone lithofacies at this site appears to be lithologically similar to that exposed on the northwest side of the fault, but no mineralization was noted at this drill site. However, the possibilities of strike-slip movement associated with this fault could imply that the mineralized zone may have been offset. As in the first hypothesis, it is not known where the copper-bearing ground waters originate.

Oxidation and Leaching

This hypothesis suggests that primary copper mineralization is localized within the shale units in the

siltstone-shale lithofacies of the upper Moya. The downward percolation of meteoric waters (rain water) may oxidized and leach the copper from the shales and deposit it in the underlying sandstone lithofacies. Another assumption this hypothesis makes is that the copper in the shales is pre-mineralization in the sandstone lithofacies.

Deposition of the copper mineralization in the sandstone lithofacies may have been controlled by two mechanisms: 1) chemical interaction of meteoric waters with interstitial calcite cements or 2) organic detritus which created a mild-reducing environment. The interaction of meteoric waters with calcite cement is favored because of the lack of carbonaceous material in the fine-to medium-grained sandstones.

The dominant copper mineralization (oxides and carbonates) is localized predominantly in the fine-to medium-grained sandstones which generally underlie the siltstone-shale lithofacies (Appendix 1 and Plates 3,4 and 5). Minor amounts of malachite and azurite are commonly localized along the fissile-bedded shales and also as fracture-fillings in the siltstone-shale lithofacies. The copper mineralization in the sandstone lithofacies appears to have a preference for the bedding-plane fractures which are lined with a carbonaceous clay. This preference could imply that

copper-bearing shales may be interbedded with the sandstone lithofacies.

The shale intervals from three drill-holes (2,3 and 10) were analyzed by x-ray fluorescence to determine their copper contents; they gave values of 205, 2564 and 375 ppm copper respectively. In providing a comparison for these values Bloom (1966) suggests that an average shale contains from 100-200 ppm copper. According to this value both shale intervals from drill-holes 3 and 10 are above average, particularly drill-hole 3 which contains about 0.25% Cu.

The irregular distribution of the copper in the shales might be explained by either of two hypotheses: 1) localized concentrations of copper initially present in the shales, or 2) certain areas within the shale units may have undergone a high degree of oxidation and leaching, which removed much of the copper. The higher degree of oxidation and leaching may be a result of higher porosity and permeability both above and below the cupiferous units.

One possible explanation for the coincident or overlapping mineral relationships is that multiple stages of copper mineralization may have occurred in this deposit and may be related to the continued flushings of the system by meteoric waters following oxidation. The replacement textures of calcite by malachite and azurite can also be

explained by this mechanism. The one major difficulty in this hypothesis is that the copper species present in the shales is unknown.

CONCLUSIONS

The copper mineralization at the Chupadero Mines area can best be described as an epigenetic, supergene deposit. Of the three hypotheses proposed for the origin of this deposit, evidence favors the oxidation and leaching of cupriferous shale by meteoric waters and deposition of copper oxides in the underlying fine-to medium-grained sandstones. These copper-bearing shales may have been derived from granitic exposures such as those located approximately two miles south-southeast of the study area during upper Virgilian time (Lochman-Balk, 1973, personal communication).

Although the fault-control hypothesis for localization and emplacement of the copper mineralization has been dismissed from further consideration, faulting still may have played an integral role in the formation of this deposit. The uplifting of a fault block containing cupriferous shales and the subsequent erosion of overburden may have exposed the copper-bearing shales to near-surface oxidizing conditions, inducing oxidation and leaching. The formation of secondary structures, fractures and joints, within and both above and below the cupriferous shales created permeable channelways for the downward percolating meteoric waters. These

channelways may also have aided in the oxidation and leaching of the copper-bearing shales.

Because the dominant copper mineralization in the Chupadero Mines area consists of malachite and azurite with minor tenorite and cuprite, this suggests relatively high concentrations of copper were present in a high f_{O_2} and f_{CO_2} environment. The formation of delafossite suggests that local concentrations of iron were present which reacted with the copper under favorable f_{O_2} and f_{CO_2} conditions.

The renewed flushings of the shales by meteoric waters may have produced the coincident and overlapping mineral relationships observed in both thin section and handspecimen. The replacement of calcite by malachite and azurite can be explained by the chemical interaction of the meteoric waters with the calcite cements in the fine-to medium-grained sandstones.

APPENDIX I

Logs of exploration drill-holes from the Chupadero Mines area. Holes drilled for New Mexico State Bureau of Mines and Mineral Resources, Summer, 1971.

SYMBOLS FOR GRAPHIC SECTIONS OF DRILL-HOLE CORES

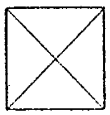

no samples

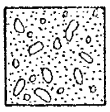

conglomerate

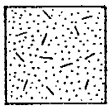

arkose

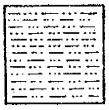

siltstone

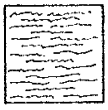

mudstone

shale

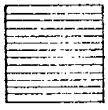

carbonaceous shale

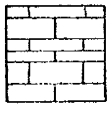

limestone

⊥ calcareous

v micaceous

△ chert

⌒ marine fossils

□ pyrite

▮ iron oxide

fracture rubble

T.D. total depth in feet

Scale of drill holes is 1″ = 5 feet unless designated otherwise

For abbreviations of formation names see Plate I

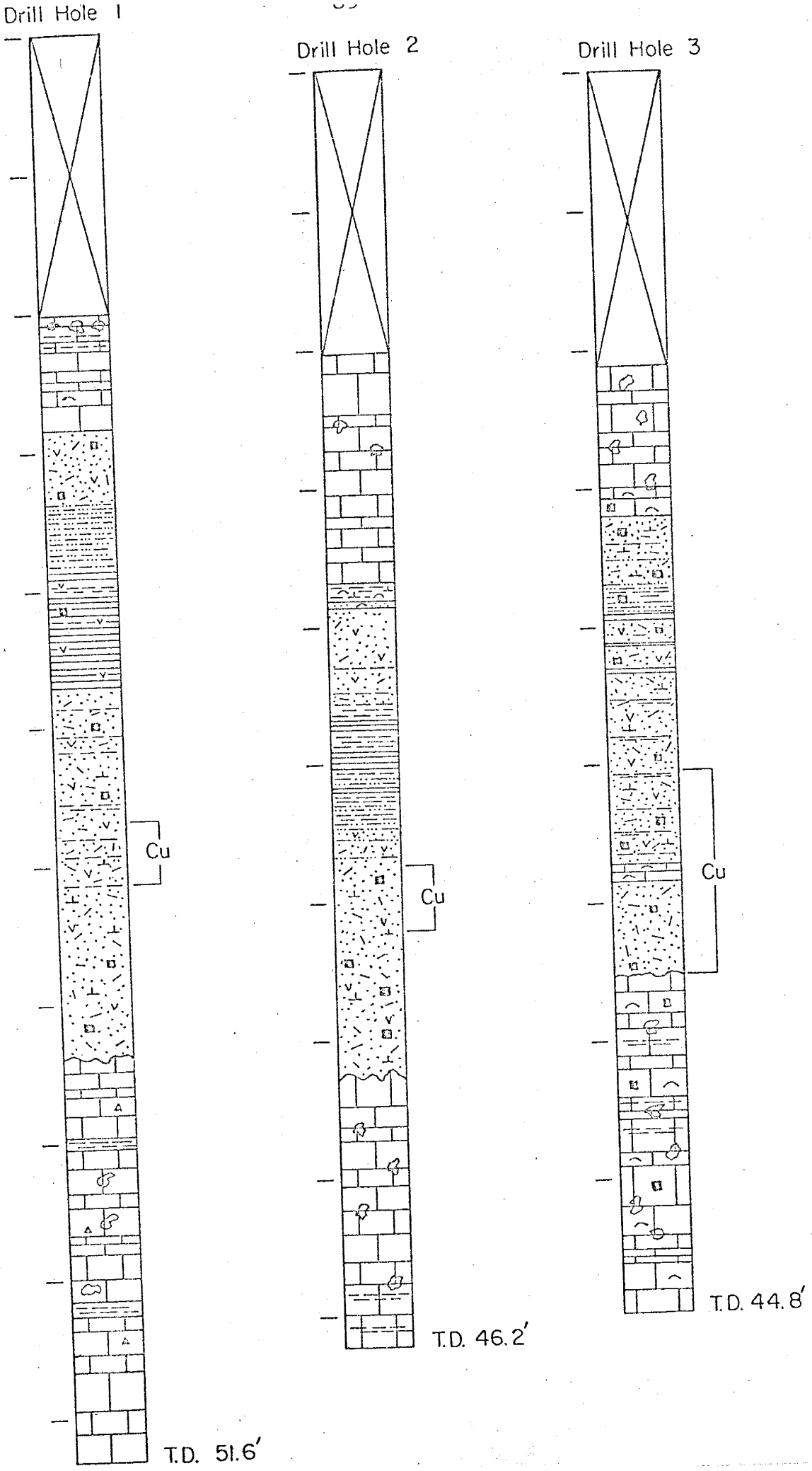
Drill Hole 1
Cu
T.D. 51.6'
Drill Hole 2
Cu
T.D. 46.2'
Drill Hole 3
Cu
T.D. 44.8'

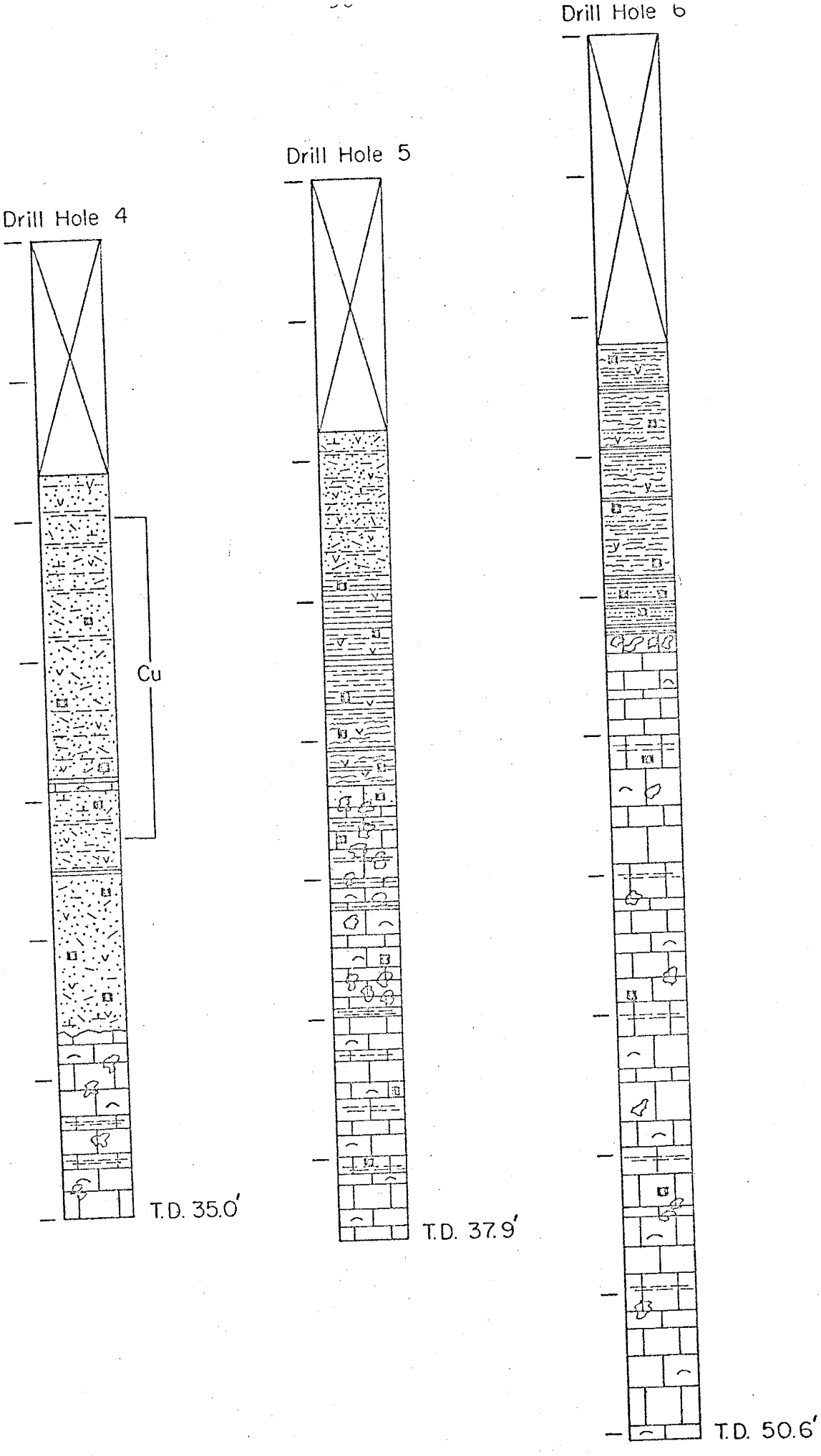
Drill Hole 4
Cu
T.D. 35.0'
Drill Hole 5
T.D. 37.9'
Drill Hole 6
T.D. 50.6'

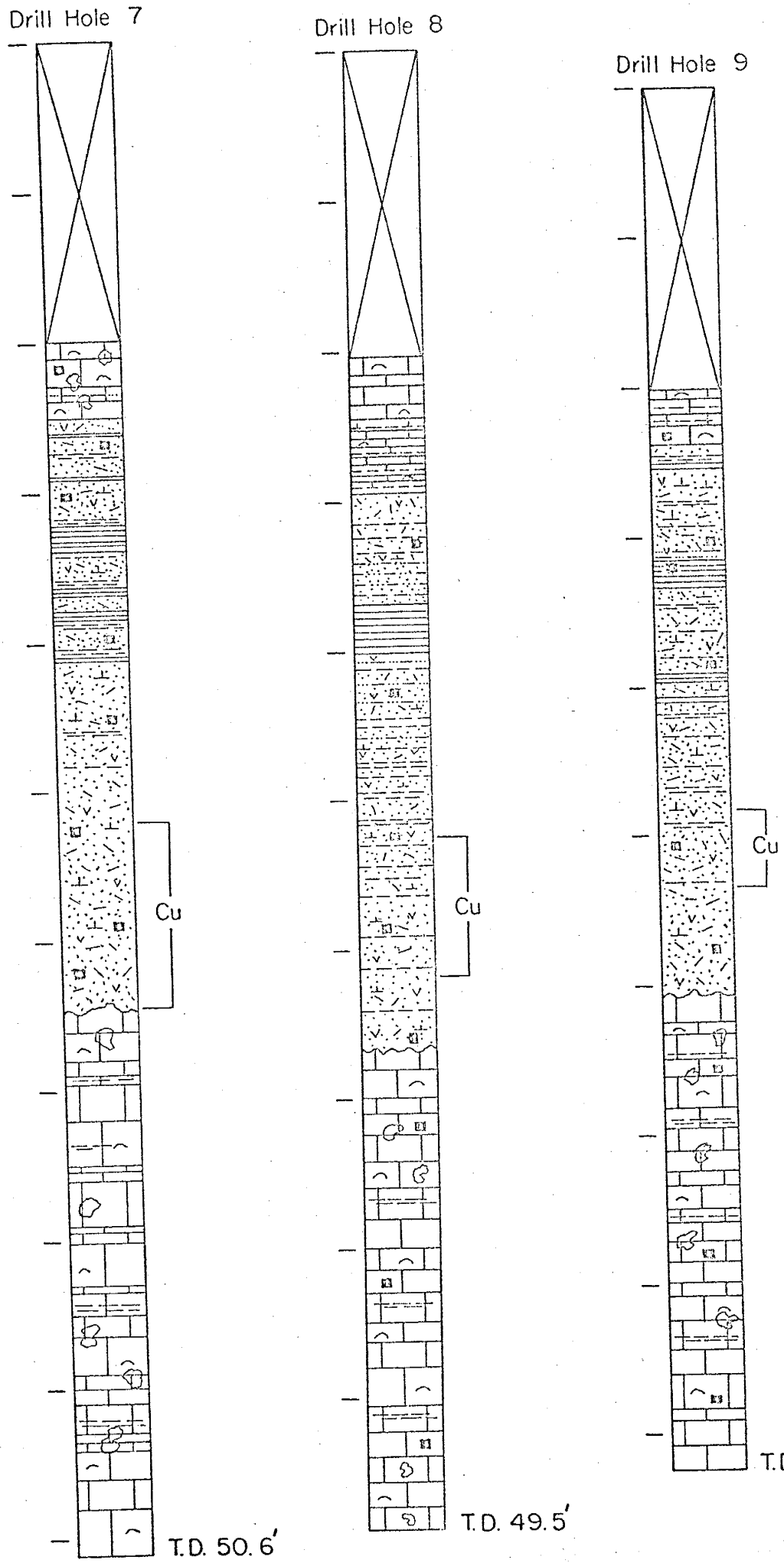
Drill Hole 7
Cu
T.D. 50.6'
Drill Hole 8
Cu
T.D. 49.5'
Drill Hole 9
Cu
T.D. 46.1'

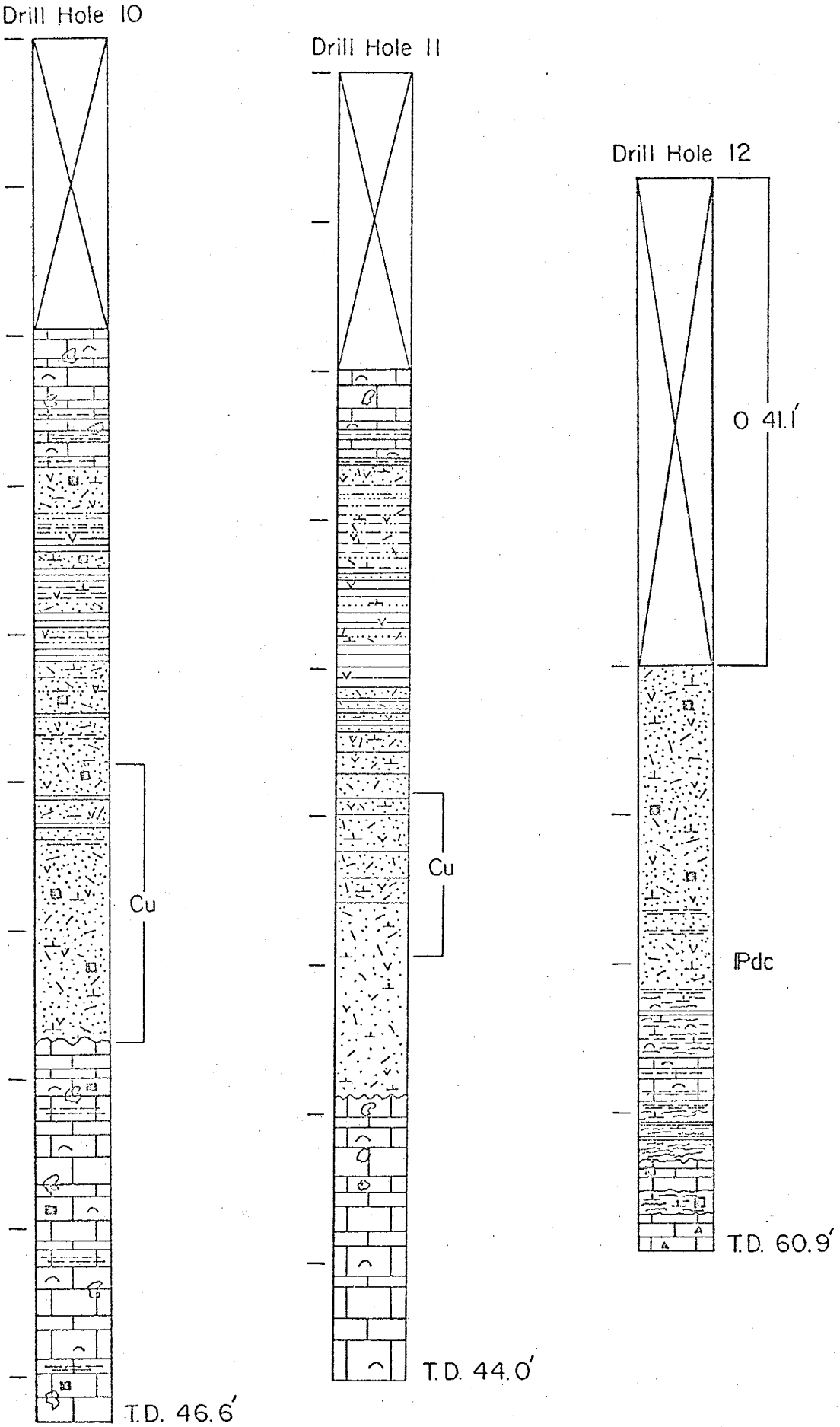
Drill Hole 10
Cu
T.D. 46.6'
Drill Hole 11
Cu
T.D. 44.0'
Drill Hole 12
O 41.1'
Pdc
T.D. 60.9'

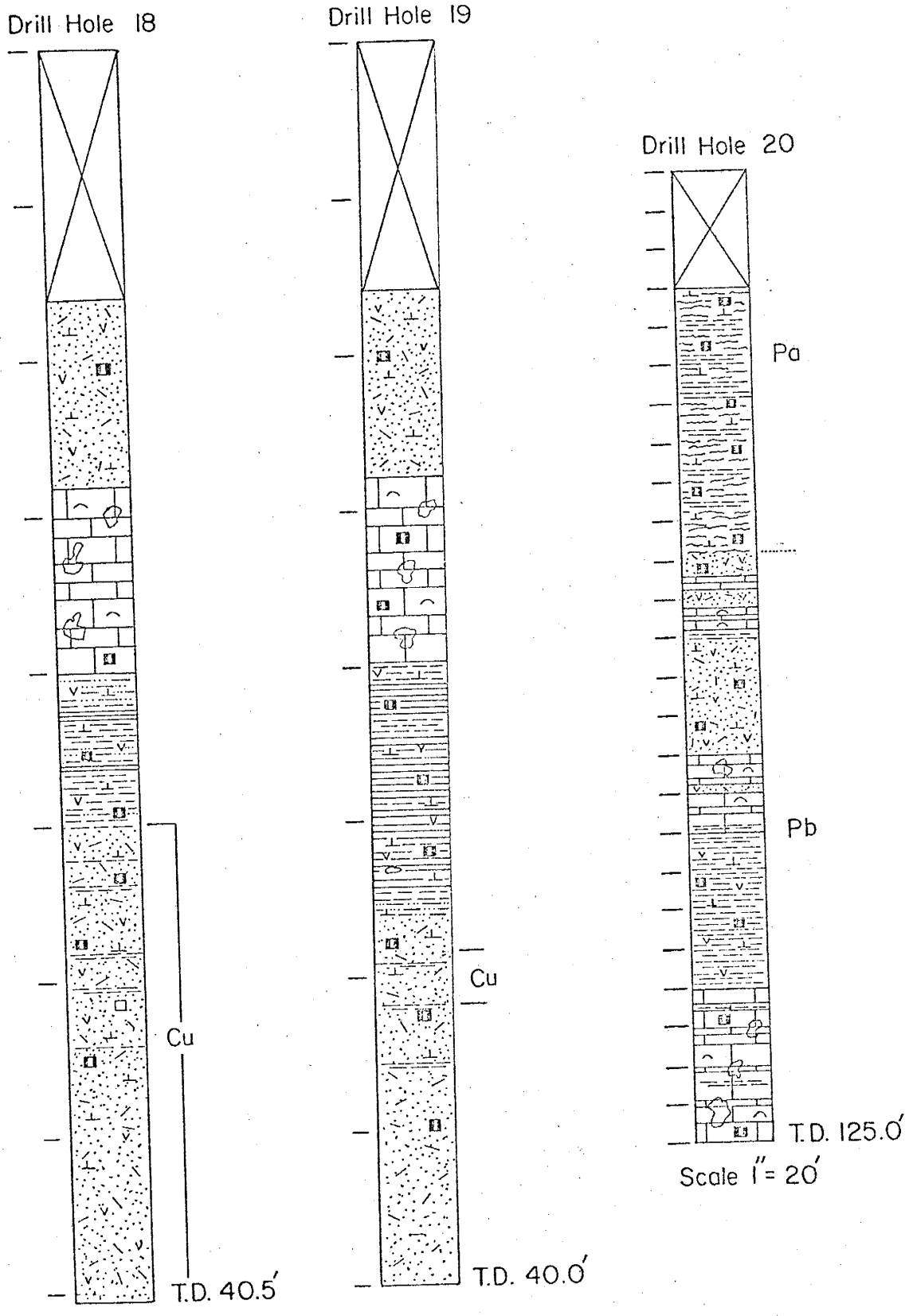
Drill Hole 18
Cu
T.D. 40.5'
Drill Hole 19
Cu
T.D. 40.0'
Drill Hole 20
Pa
Pb
T.D. 125.0'
Scale 1" = 20'

Drill Hole 21

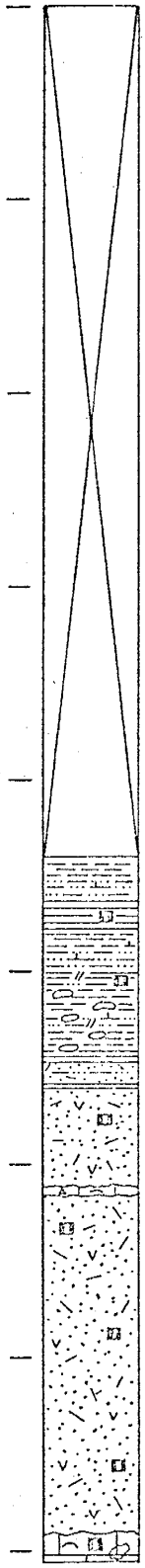

T.D. 40.1'

Drill Hole 22

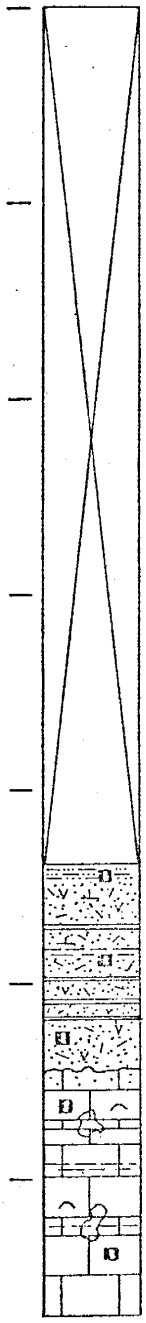

T.D. 33.5'

APPENDIX II

Classification procedure and petrographic analysis of the clastic sediments, with particular emphasis placed on the sandstone lithofacies of the upper member of the Moya Formation.

Schematic diagram linking Folk's and Dott's classification.

Composition of the sandstones was determined by petrographic analysis of thin sections cut from drill-hole cores. A classification adapted from Koehn (1972, presented on following page) which combines Folk's 1968 sandstone classification with Dott's 1964 classification was employed. This scheme was selected because it includes a consideration of the matrix as well as the particle compositions. The arenite and wacke boundary in this classification was placed at an arbitrary 25 percent matrix content by Koehn (1972).

During the examination of the thin sections all identifiable components were calculated to the nearest percent, including cement although it did not enter into the classification framework. In order to classify the rocks, the original percentages of quartz, feldspar and rock fragments were recalculated to 100 percent to obtain a point (a compositional name) on Folk's ternary classification scheme. This point was then compared to the percentage of matrix originally calculated in order to determine whether the rock belonged to the arenite or wacke group.

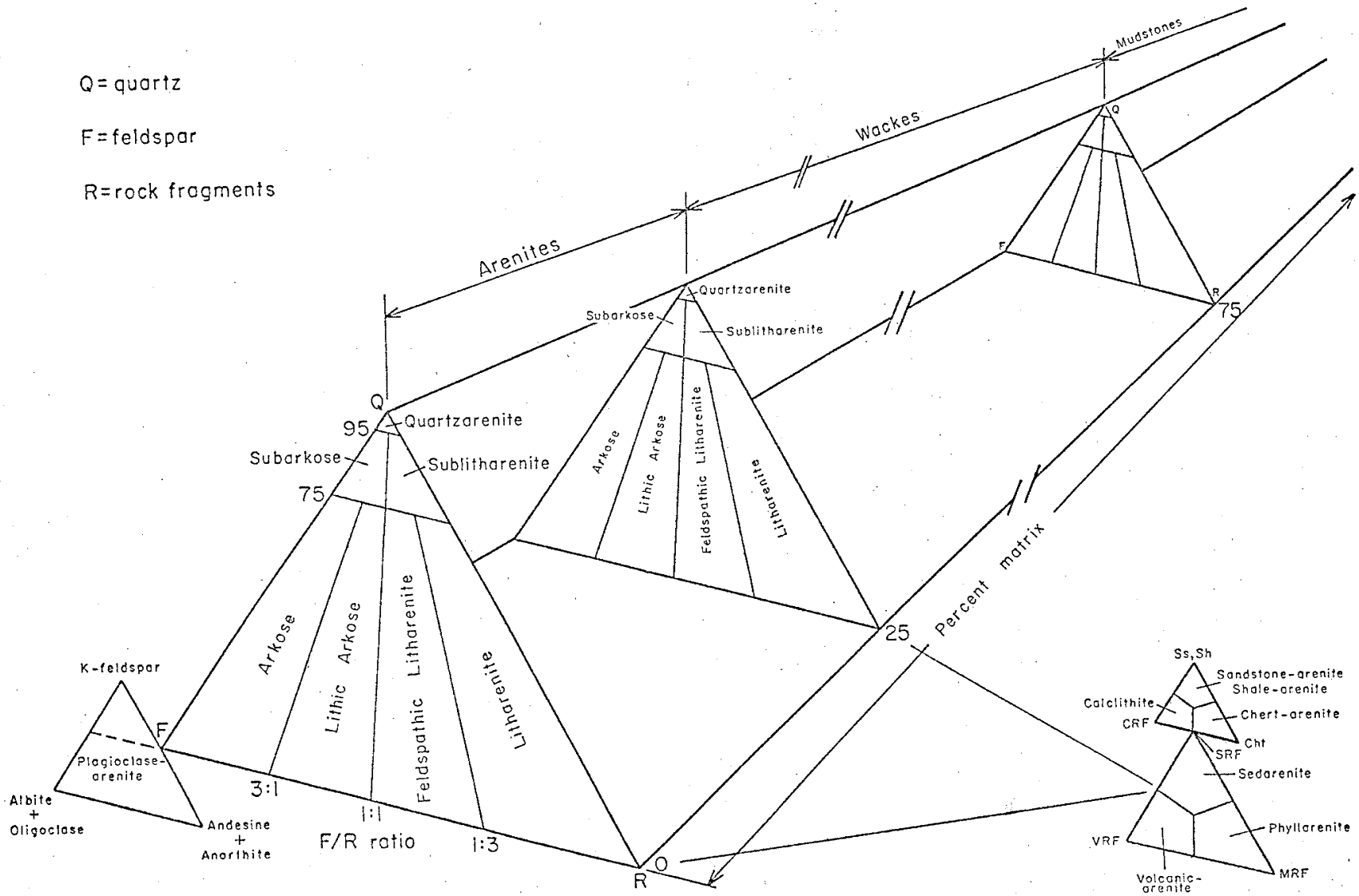

Schematic diagram linking Folk's and Dott's classification.

BIBLIOGRAPHY

Allen, J. R. L., 1965, Studies in fluviatile sedimentation: a comparison of fining upwards cyclothems, with special reference to coarse member composition and interpretation. Jour. Sed. Petrology, v. 40, p. 298-323.

Bates, C. C., 1953, Rational theory of delta formation: Amer. Assoc. Petroleum Geologists, Bull., v. 37, p. 2119-2162.

Bloom, H., 1966, Geochemical exploration as applied to Copper-Molybdenum deposits, in Geology of the Porphyry Copper Deposits Southwestern North America, S. R. Titley and C. L. Hicks, eds.: University of Arizona Press, Tuscon, Arizona, p. 111-122.

Conybeare, C. E. B., and Crook, K. A. W., 1968, Manual of Sedimentary Structures: Dept. of Nat. Devel. Bur. Mines Resources, Geology and Geophysics, Bull. 102, 327 p.

Dott, R. H., Jr., 1964, Wacke, gray wacke and matrix-What approach to immature sandstone classification?: Jour. Sed. Petrology, v. 35, p. 625-632.

Folk, R. L., 1968, Petrology of Sedimentary Rocks: Austin, Tex., Hemphill's Pub., p. 124.

Garrels, R. M., and Christ, C. L., 1965, Solutions, Minerals, and Equilibria: New York, Harper and Row, 450 p.

Hambleton, A. W., 1959, Interpretation of the paleoenvironment of several Missourian carbonate sections in Socorro County, New Mexico, by carbonate fabrics: Unpublished Masters Thesis, New Mex. Inst. Min. and Tech., 87 p.

Koehn, M. A., 1972, Petrographical and paleoenvironmental study of the Glorieta sandstone near Rowe, New Mexico: Unpublished Masters Thesis, New Mex. Inst. Min. and Tech., 132 p.

Krauskopf, K. B., 1967, Introduction to Geochemistry: New York, N. Y., McGraw-Hill Book Co., 721 p.

Krumbein, W. C. and Sloss, L. L., 1963, Stratigraphy and Sedimentation: W. H. Freeman and Company, San Francisco, 660 p.

Lasky, S. G., 1932, The ore deposits of Socorro County, New Mexico: New Mex. State Bur. Mines Mineral Resources Bull. 8, p. 136.

Needham, C. E., and Bates, R. L., 1943, Permian type section in central New Mexico: Geol. Soc. America, Bull., v. 54, p. 1653-1668.

Pettijohn, F. J., Potter, P. E., and Siever, R., 1972, Sand and Sandstone: New York-Heidelberg-Berlin, Springer-Verlag, 618 p.

Rejas, A., 1965, Geology of the Cerros de Amado area Socorro County, New Mexico: Unpublished Masters Thesis, New Mex. Inst. Min. and Tech., 128 p.

Robie, and Waldbaum, 1968, Thermodynamic properties of minerals and related substances: U.S.G.S. Bull. 1259, 256 p.

Rossini, F. D., Wagman, D. D., Evans, W. H., Levine, S., Jaffe, I., 1969, Selected values of chemical thermodynamic properties: U. S. Department of Commerce, National Bureau of Standards, Technical Note 270-4, p. 88.

Soule, J. H., 1956, Reconnaissance of the "Red Bed" copper deposits in southeastern Colorado and New Mexico: U. S. Bur. Mines Inf. Circ. 7740, p. 57-65.

Thompson, M. L., 1942, Pennsylvanian system in New Mexico: New Mex. State Bur. Mines Mineral Resources, Bull. 17, 85 p.

Wilpolt, R. H., MacAlpin, A. J., Bates, R. L., and Vorbe, G., 1946, Geologic map and stratigraphic sections of Paleozoic rocks of Joyita Hills, Los Pinos Mountains and northern Chupadera Mesa, Valencia, Torrence, and Socorro Counties, New Mexico: U. S. Geol. Survey, Oil Gas Inv. Prelim. Map 61.

Wilpolt, R. H., and Wanek, A. A., 1951, Geology of the region from Socorro and San Antonio east to Chupadera Mesa, Socorro County, New Mexico: U. S. Geol. Survey, Oil Gas Inv. Prelim. Map 121.

Zalazinskii, A. G., Balakirev, V. F., Chebotaev, N. M., and Chufarov, G. S., 1969, Thermodynamic analysis of the reduction, dissociation, and formation from the elements and oxides of $CuAlO_2$, $CuCrO_2$, and $CuFeO_2$: Russ. Jour. Inorg. Chem.

This thesis is accepted on behalf of the faculty of the Institute by the following committee:

Karl Vander Linden

Christina L. Balk

Irene E. Kotkowski

Richard C Beane

Date Sept. 4, 1973

Drill Hole 13

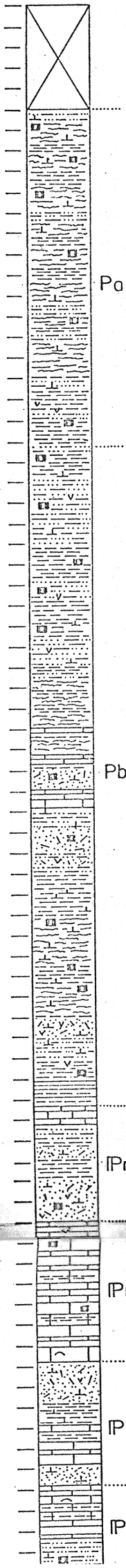

Drill Hole 14

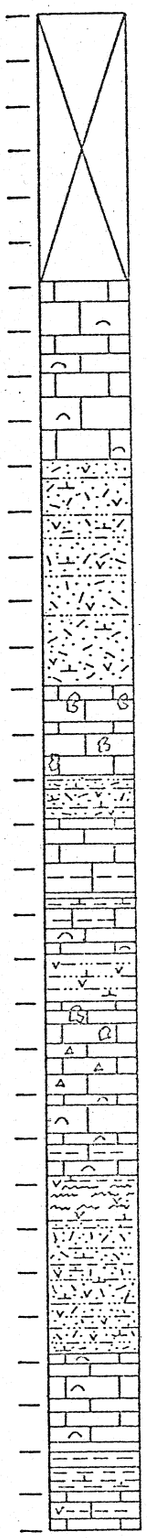

Scale 1" = 20'

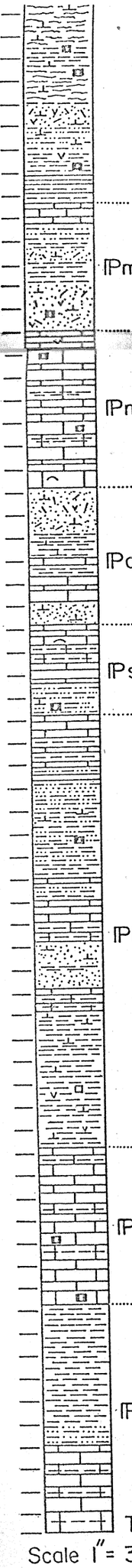

Scale 1" = 30'

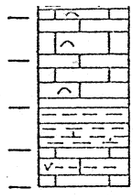

Scale 1" = 20'

Drill Hole 15

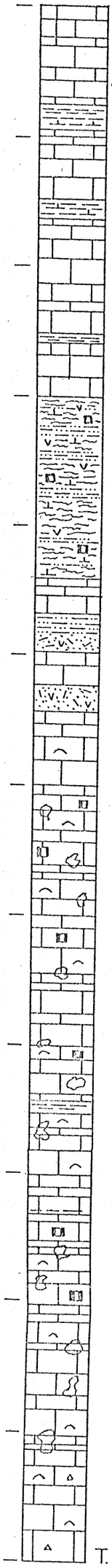

T.D. 60.0′

Drill Hole 16

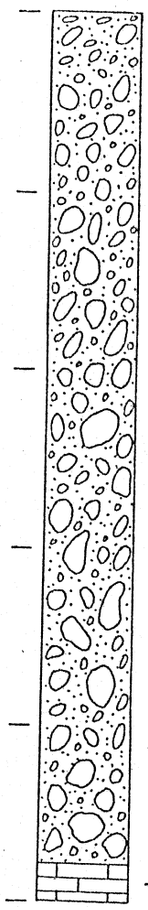

T.D. 25.0′

Drill Hole 17